Modeling and Analysis of Air-Ground Integrated Networks With Flexible Beam Coverage

Na Deng, *Member, IEEE*, Haichao Wei, and Martin Haenggi, *Fellow, IEEE*

Abstract

Air platforms, such as unmanned aerial vehicles, airships, and balloons are expected to complement traditional ground networks to provide flexible coverage solutions. However, most existing models for air-ground integrated networks (AGINs) neglect the spatial dependence caused by the complementary deployment of the aerial and ground nodes. Accordingly, in this paper, we propose two AGIN models with horizontal dependence that differ in the vertical dimension, namely uniformly independent altitudes and location-dependent altitudes. The air platforms serve as aerial base stations, distributed as a marked Poisson hole process, and provide flexible beam coverage through varying altitudes. Under this setup, we propose a region-based user association scheme and derive the association probabilities as well as the serving distance distributions of an arbitrarily located user. Considering Nakagami fading and air-to-ground propagation properties, we characterize the signal-to-interference ratio and area spectral efficiency for each model. Using the proposed analytical framework, we demonstrate the importance of deploying the air platforms more sensibly to provide targeted services and flexible beam coverage in reducing the load of base stations and improving the user coverage and network capacity performance.

Index Terms

N. Deng is with the School of Information and Communication Engineering, Dalian University of Technology (DLUT), Dalian, 116024, China (e-mail: dengna@dlut.edu.cn). H. Wei is with the School of Information Science and Technology, Dalian Maritime University, Dalian 116026, China (e-mail: weihaichao@dlmu.edu.cn). M. Haenggi is with the Dept. of Electrical Engineering, University of Notre Dame, Notre Dame 46556, USA (e-mail: mhaenggi@nd.edu).

Part of this work was presented at the 2021 IEEE Wireless Communications and Networking Conference (WCNC'21) [1]. This work was supported by the National Natural Science Foundation of China under Grant 62201115 and 61701071, by the Natural Science Foundation of Liaoning Province (2021-MS-112), by the Fundamental Research Funds for the Central Universities (DUT21JC04), and by the US National Science Foundation under Grant 2007498.

Air-ground integrated networks, spatial dependence, aerial base stations, Poisson hole process, SIR distribution.

I. Introduction

A. Motivation

To meet the increasing requirements of ubiquitous coverage and diverse services in future B5G/6G networks, air-ground integrated networks (AGINs) provide a promising architecture for ubiquitous and reliable service for anyone, anywhere, at any time [2–4]. Due to the capability of flexible deployment, avoiding obstacles, and improving the possibility of line-of-sight (LOS) links to ground users, unmanned aerial vehicles (UAVs) have recently been proposed to serve as aerial base stations (ABSs). This means the UAV tier forms a complementary access layer for the existing terrestrial network, which inevitably leads to correlation in the aerial and terrestrial layers. For instance, aerial nodes are deployed in regions with poor or even no service, e.g., the cell edge of the ground BSs (GBSs) or emergency areas with damaged or otherwise unavailable infrastructure, to provide flexible and temporary coverage service. These typical scenarios have the common feature that the air platforms are usually deployed in specific regions where GBSs provide insufficient service rather than independently of the GBSs. Hence there is *horizontal dependence* between the locations of GBSs and UAVs.

While the LOS propagation of ABSs provides good signal strength to their users, it causes serious interference to the users served by other access points (GBSs and UAVs). To address this problem, a possible method is to use a directional antenna array for UAVs to form a downward beam. The region of such vertical beam coverage depends on the UAV's altitude and the beamwidth of the main lobe. It is straightforward that it increases with the altitude, which allows more users access. But at the same time, the desired signal strength decreases with the serving distance. As a consequence of this trade-off, there exists an optimum altitude and an optimum distance from GBSs in the UAV deployment. This deployment determines the UAV's altitude (also the beam coverage) as a function of the distance from its nearest GBS in the horizontal dimension (termed *vertical dependence*). Such vertical dependence is an important feature of the spatial configuration of network nodes induced by the integration of the aerial nodes, which has not been investigated yet. This type of dependence is inextricably linked with the UAV deployment, the coverage of the whole AGINs, as well as the user-perceived

performance. As a consequence, models for AGINs accounting for both the horizontal and vertical dependence should be devised and analyzed to reveal the impacts of different UAV deployment schemes on the trade-offs between the link- and network-level performances. The results provide guidelines on how to achieve an effective integration between aerial and terrestrial network layers.

B. Related Work

Due to the capability of accurately capturing the irregularity and variability of the spatial network topology, stochastic geometry has been widely used to establish various terrestrial network models and analyze the key performance metrics [5]. Recently, it has also been applied in aerial networks by capturing the salient aerial properties to characterize different performance metrics. In [6, 7], a homogeneous Poisson point process (PPP) is used to model the spatial distribution of the GBSs, and the expected signal-to-interference-plus-noise ratio (SINR) as well as the signal-to-interference ratio (SIR) distribution for the typical UAV are derived to investigate how the antenna pattern of GBSs affect the GBS-UAV link. In [8–10], a non-orthogonal multiple access (NOMA) scheme is adopted for both aerial and terrestrial users, and stochastic geometry is utilized to model their spatial randomness and analyze the SINR distribution and average rate and show the gain achieved by the NOMA schemes in different scenarios. In these works, the UAVs act as cellular-connected aerial users, and different from them, the articles of [11–15] focus on the case where UAVs act as the aerial access points to provide service for terrestrial users. However, merely single-tier aerial networks are considered, disregarding the coexistence between the aerial and terrestrial networks.

In the context of AGIN modeling and analysis, the authors in [16] focus on a scenario where a single UAV is deployed over a disk-shaped malfunction region within which GBSs are inoperational, distributed according to a PPP. Under this setup, a user-centric cooperative scheme is proposed for users in the malfunction region and the SIR distribution as well as the normalized spectral efficiency are analyzed with the tools from stochastic geometry. In [17], the UAVs are again deployed over a disk, following a binomial point process, and coexist with GBSs modeled by an independent PPP in the plane. Based on this model, the SIR distribution and area spectral efficiency are analyzed by considering a probabilistic LOS and non-line-of-sight (NLOS) propagation model. The same model is adopted in [18], where the SIR distribution is investigated

by introducing the backhaul links between UAVs and GBSs. Extending the UAV deployment to an (elevated) plane at a fixed altitude, the authors in [19–21] model the (projection) locations of UAVs and GBSs as two independent PPPs to investigate the interplay between UAVs and GBSs on different key performance metrics, such as the SIR/SINR distribution, achievable rate and medium access probability, etc. Furthermore, considering different altitudes for different types of ABSs, multiple independent PPPs are used to model the projection locations of multi-layer ABSs in [22].

Although there are many works that proposed models for AGINs to capture the variability and randomness of the locations of network nodes, the spatial correlation between the aerial and terrestrial network layers is rarely considered. In [23, 24], the locations of UAVs follow a clustered point process around the GBSs to serve the hotspot or post-disaster recovery regions, which shows the spatial attraction correlation between UAVs and GBSs. Another type of spatial exclusion correlation is considered in [25, 26], where GBSs are distributed according to a PPP and UAVs are deployed in the cell edge region, and bounds on the SIR/SINR distribution of users associated with UAVs and GBSs are provided. However, they both assumed that all UAVs hover at a fixed common altitude, neglecting the vertical dependence present in practical scenarios.

In summary, while previous works in modeling and evaluating AGINs have provided solid design guidelines, important issues remain unexplored. To our best knowledge, no prior work has considered the spatial dependence between the aerial and ground tiers taking the flexibility of air platforms (e.g., location-dependent altitudes) and vertical coverage (e.g., directional downward beams) into account, which is addressed comprehensively in this paper.

C. Contributions

- Different from the current mutually independent models for ground and aerial tiers, we propose two new AGIN models with horizontal dependence that differ in the vertical dimension, namely uniformly independent altitudes (Model 1) and location-dependent altitudes (Model 2). Since these models capture the dependence between the tiers, they are more accurate than previously proposed models.
- To fully exploit the agility of the UAVs and mitigate the interference, we propose a flexible beam coverage approach for UAVs equipped with a directional antenna array, which is tied to the UAVs' altitudes and the beamwidth of the main lobe.

- We propose a region-based user association scheme and derive the association probabilities for the typical user accessing the ground and aerial tiers, respectively.
- To facilitate the performance analysis, we provide two key intermediate results: the horizontal serving distance distributions and altitude distributions for the two models.
- We analyze the signal-to-interference ratio (SIR) distribution and the area spectral efficiency for the two models with Nakagami fading and air-to-ground propagation properties. A modified Weibull distribution and an approximate distribution for the serving UAV's altitude are adopted to provide simple yet highly accurate analytical expressions.
- We use the Möbius homeomorphic distance [27] to quantify the accuracy of the analytical results under the proposed approximations, which match the simulations well. It is also shown that a better performance can be obtained if the UAVs are deployed smartly, i.e., by keeping a certain distance from the GBSs or hovering at an appropriate altitude.

II. System Model

A. Network Model

We consider an air-ground integrated network (AGIN) composed of GBSs and UAVs sharing the same spectrum. The locations of the GBSs follow a homogeneous PPP $\Phi_{\rm g} = \{x_1, x_2, \ldots\} \subset \mathbb{R}^2$ of density $\lambda_{\rm g}$. Each GBS is equipped with an omnidirectional antenna[1] in the horizontal plane, and the transmit power is $\mu_{\rm m}$. The potential UAVs follow a marked PPP $\widetilde{\Phi}_{\rm u} = \{(y, h_y)\}$ [29, Def. 7.1], where the points $y \in \mathbb{R}^2$ constitute an unmarked point process of density $\widetilde{\lambda}_{\rm u}$ corresponding to the locations of UAVs projected to the ground plane and the h_y are the marks specifying the hovering altitudes. The locations of the UAVs actually deployed depend on the locations of the GBSs and are obtained by deleting certain points in $\widetilde{\Phi}_{\rm u}$ as specified in Sec. II-B. Each UAV has a directional antenna array to provide flexible beam coverage downward, and the transmit power is $\mu_{\rm u}$. The antenna gain function with the sectorized model is

$$G(\phi) = \begin{cases} G_{\rm m} & \text{if } |\phi| \le \psi_{\rm m} \\ G_{\rm s} & \text{otherwise,} \end{cases} \tag{1}$$

where $G_{\rm m}$ and $G_{\rm s}$ are antenna gains of the main and side lobes, respectively, $\psi_{\rm m}$ is the half of the half-power beamwidth (HPBW), and ϕ is the direction angle of the transmit signal off

[1]It is straightforward to analyze the multi-antenna scenarios via the widely-used sectorized antenna pattern model [28].

the baseline downward direction. As a result, the beam coverage of the UAV (y, h_y) is a disk centered at y with radius $R_y = h_y \tan \psi_{\rm m}$ formed by its main lobe beam.

As discussed in [30], the UAVs have a high chance to provide LOS propagation to ground users, resulting in lower signal attenuation than NLOS propagation. To capture this unique feature, a common probabilistic model is adopted in which the LOS probability of the channel between the UAV and a user with the horizontal distance r and vertical distance u is [30]

$$P_{\rm L}(r,u) = \frac{1}{1+\nu\exp(-\kappa(\frac{180}{\pi}\arctan(u/r)-\nu))}, \tag{2}$$

where ν and κ are constants that allow an adjustment to different propagation environments. The NLOS probability is $P_{\rm N}(r,u) = 1 - P_{\rm L}(r,u)$. From (2), it can be seen that the LOS probability increases with the elevation angle, which is consistent with the real situation. Different path loss exponents are applied to different links, denoted as $\alpha_{\rm L}$ and $\alpha_{\rm N}$, for LOS and NLOS channels, respectively, where $2 < \alpha_{\rm L} \leq \alpha_{\rm N}$. The random path loss function associated with the link from UAV (y, h_y) to the origin is given by

$$\ell_{\rm u}(y) = \begin{cases} \left(\|y\|^2 + h_y^2\right)^{-\alpha_{\rm L}/2} & \text{w.p. } P_{\rm L}(\|y\|, h_y) \\ \left(\|y\|^2 + h_y^2\right)^{-\alpha_{\rm N}/2} & \text{w.p. } P_{\rm N}(\|y\|, h_y), \end{cases} \tag{3}$$

where all $\ell_{\rm u}(y)_{(y,h_y)\in\tilde{\Phi}_{\rm u}}$ are independent. For the ground-to-ground links, both the transmitters and receivers are on the ground plane and the link is always assumed NLOS with a power path loss law $\ell_{\rm g}(x) = \|x\|^{-\alpha_{\rm N}}$. Nakagami fading is adopted to model the small-scale fading, and the power fading coefficient follows a gamma distribution $\mathrm{Gamma}(M, 1/M)$, where $M = M_{\rm L} > 1$ for the LOS link and $M = M_{\rm N} = 1$ for the NLOS link (i.e., Rayleigh fading). The power fading coefficients are mutually independent and also independent of $\Phi_{\rm g}$ and $\widetilde{\Phi}_{\rm u}$.

B. AGIN Models with Dependence

Owing to the unique attributes (such as flexibility and 3D deployment) of UAVs, the spatial dependence between the aerial- and terrestrial-network tiers (i.e., the inter-tier dependence) becomes more intricate than in traditional ground networks. Therefore, we propose two AGIN models that capture the inter-tier dependence in the horizontal and vertical dimensions, corresponding to different UAV deployments.

In the horizontal dimension, since users at the cell center mostly experience a high quality of service from GBSs, an effective and economic way is to deploy UAVs over the cell edge to

assist GBSs in improving the performance of cell edge users. Accordingly, each GBS is assumed to have an exclusion disk with radius D centered at the location of the GBS, and UAVs are deployed outside these disks, which significantly reduces the interference from UAVs to the users served by GBSs. Under this setup, the UAVs follow a *marked Poisson hole process* (MPHP), expressed by

$$\Phi_{\mathrm{u}} = \{(y, h_y) \in \widetilde{\Phi}_{\mathrm{u}} \colon \min_{x \in \Phi_{\mathrm{g}}} \|y - x\| > D\}, \tag{4}$$

where the projections of the UAVs form a PHP [29, Example 3.7] with density $\lambda_{\mathrm{u}} = \widetilde{\lambda}_{\mathrm{u}} e^{-\lambda_{\mathrm{g}} \pi D^2}$, capturing the dependence between GBSs and UAVs in the horizontal dimension.

In the vertical dimension, to capture different deployment schemes, we propose the following two models for UAV altitudes, where $h_{\min}$ and $h_{\max}$ are the minimum and maximum allowable altitudes as regulated by the government and industrial association [31].

1) Uniformly Independent Altitudes (Model 1): The altitudes of the UAVs are uniformly independent random variables with identical probability density function (PDF) $f(u) = \frac{1}{h_{\max} - h_{\min}}$, $u \in [h_{\min}, h_{\max}]$, which are also independent of the projected locations of UAVs. When $h_{\max} = h_{\min} = h_{\mathrm{f}}$, the altitudes of the UAVs are the same and this model reduces to the special case of equal deterministic altitudes.

2) Location-Dependent Altitudes (Model 2): Considering that UAVs with a lower altitude can provide stronger signals to their users but lead to smaller beam coverage regions, we also consider a location-dependent model case where each UAV's altitude is a non-decreasing function of the horizontal distance to its nearest GBS. By sensibly choosing this function, the trade-off between the per-user performance and the total coverage region of UAVs can be well managed. This model induces a dependence between GBSs and UAVs in the vertical dimension. To make sure the UAVs significantly enhance the network performance, the desired altitude $\tilde{h}_y$ of the UAV over location y is determined such that the received power at y from the UAV is ζ times larger than that received from the nearest GBS on average, where ζ is a design parameter. Mathematically, letting $z = \min_{x \in \Phi_{\mathrm{g}}} \|y - x\|$, we have $\mu_{\mathrm{u}} \tilde{h}_y^{-\alpha_{\mathrm{L}}} = \zeta \mu_{\mathrm{g}} z^{-\alpha_{\mathrm{N}}}$. Since $\tilde{h}_y$ may fall outside the interval $[h_{\min}, h_{\max}]$, it will be clipped to this interval. So h_y is given by

$$h_y = \max\{\min\{h(z), h_{\max}\}, h_{\min}\}, \tag{5}$$

where $h(z) \triangleq (\frac{\mu_{\mathrm{u}}}{\mu_{\mathrm{g}} \zeta})^{1/\alpha_{\mathrm{L}}} z^{\alpha_{\mathrm{N}}/\alpha_{\mathrm{L}}}$. Fig. 1 illustrates this network scenario, the PHP realization for UAV projections as well as Model 2 with flexible beam coverage, jointly considering horizontal

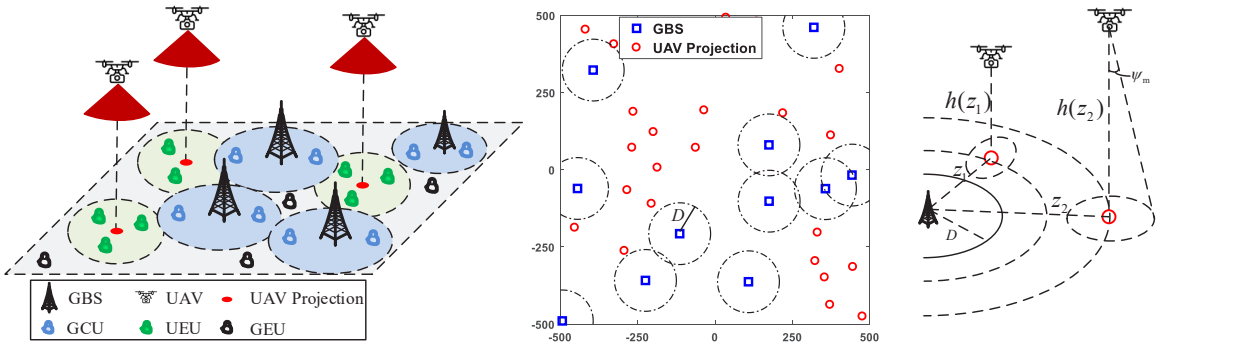

(a) An example scenario

(b) A PHP realization for UAV projections with λ_g=10^{-5} m^{-2}, λ_u=2.2×10^{-5} m^{-2}, D=100 m

(c) Location-dependent altitude (Model 2)

Fig. 1. Network architecture of an AGIN composed of GBSs and UAVs and its model with inter-tier dependence shown in (a). The circles around the GBSs indicate their exclusion regions, the circles around the UAV projections are their coverage regions, and the horizontal and vertical dependence between the UAVs and GBSs are shown in (b) and (c), respectively.

and vertical dependences.

C. User Association and SIR Analysis

Due to the exclusion regions of GBSs and the beam coverage of UAVs, the plane is divided into three parts, and we propose a region-based user association scheme. Specifically, we denote by $\mathcal{C}_1$, $\mathcal{C}_2$ and $\mathcal{C}_3$ the union of the exclusion regions of GBSs, the union of the beam coverage regions of UAVs but excluding $\mathcal{C}_1$ and the remaining region, respectively, i.e.,

$$\mathcal{C}_1 = \bigcup_{x\in\Phi_{\rm g}} b\big(x, D\big), \quad \mathcal{C}_2 = \bigcup_{(y,h_y)\in\Phi_{\rm u}} b\big(y, h_y \tan\psi_{\rm m}\big) \setminus \mathcal{C}_1, \quad \mathcal{C}_3 = \mathbb{R}^2 \setminus \big(\mathcal{C}_1 \cup \mathcal{C}_2\big), \tag{6}$$

where $b(x, r)$ denotes the disk centered at x with radius r. Then, a user lying in $\mathcal{C}_1$ or $\mathcal{C}_3$ is associated with its nearest GBS, called a ground central user (GCU) or ground edge user (GEU), respectively, and a user lying in $\mathcal{C}_2$ is served by the UAV with the smallest horizontal distance and called a UAV edge user (UEU).

We focus on an interference-limited network and consider the typical user at the origin o, which is the typical user for an arbitrary stationary point process of users that is independent of the GBSs and UAVs. If the typical user is a GCU or GEU, its serving GBS is denoted by x_0, and the typical user suffers from two types of interference: one from the other GBSs, and the other from all UAVs. If the typical user is a UEU, its serving UAV is denoted by (y_0, h_{y_0}),

and the user also suffers from two types of interference: one from all GBSs and the other from the other UAVs. We further assume that all BSs and UAVs are fully loaded to characterize the worst-case SIR-based coverage performance, and thus the interfering BSs (or UAVs) are the ones in $\Phi_{\rm g}$ (or $\Phi_{\rm u}$) except the serving BS (or UAV). For notational simplicity, we let $\Phi_{\rm g}^{!} = \Phi_{\rm g} \setminus \{x_0\}$, $\Phi_{\rm u}^{!} = \Phi_{\rm u} \setminus \{(y_0, h_{y_0})\}$, and we give a unified expression for the SIR at the typical user as

$$\mathrm{SIR} = \begin{cases} \frac{\mu_{\rm g} g_{x_0} \ell_{\rm g}(x_0)}{I_{\rm g}+I_{\rm u}} & \text{if } o \in \mathcal{C}_1 \cup \mathcal{C}_3, \\ \frac{\mu_{\rm u} G_{\rm m} g_{y_0} \ell_{\rm u}(y_0)}{I_{\rm g}+I_{\rm u}} & \text{if } o \in \mathcal{C}_2, \end{cases} \tag{7}$$

where $I_{\rm g}$ and $I_{\rm u}$ denote the two types of the interference, given by

$$I_{\rm g} = \begin{cases} \sum_{x \in \Phi_{\rm g}^{!}} \mu_{\rm g} g_x \ell_{\rm g}(x) & \text{if } o \in \mathcal{C}_1 \cup \mathcal{C}_3, \\ \sum_{x \in \Phi_{\rm g}} \mu_{\rm g} g_x \ell_{\rm g}(x) & \text{if } o \in \mathcal{C}_2, \end{cases}$$

$$I_{\rm u} = \begin{cases} \sum_{(y,h_y) \in \Phi_{\rm u}} \mu_{\rm u} G(\phi_y) g_y \ell_{\rm u}(y) & \text{if } o \in \mathcal{C}_1 \cup \mathcal{C}_3, \\ \sum_{(y,h_y) \in \Phi_{\rm u}^{!}} \mu_{\rm u} G(\phi_y) g_y \ell_{\rm u}(y) & \text{if } o \in \mathcal{C}_2, \end{cases} \tag{8}$$

and ϕ_y presents the direction angle of the transmit signal from the UAV (y, h_y) to the typical user off the baseline vertically downward direction, and g_x and g_y are the power fading coefficients from GBS x and UAV (y, h_y), respectively, to capture the small-scale fading effect as described in Sec. II-A. Although the SIRs of GCUs and GEUs have the same expressions, the spatial distributions of the interfering nodes and the desired signal strength are different due to the different locations in the cell. The main symbols and parameters are summarized in Table I, and default values are given where applicable.

III. Association Probability

In this section, for each of the proposed AGIN models, we provide the association probabilities of the typical user (the probabilities of the typical user lying in $\mathcal{C}_1$, $\mathcal{C}_2$ and $\mathcal{C}_3$), which also reflects the fractions of GCUs, UEUs, and GEUs in the network.

A. AGIN Model with Uniformly Independent Altitudes (Model 1)

In this model, each UAV has an altitude h_y with PDF $f(u) = 1/(h_{\max} - h_{\min}), u \in [h_{\min}, h_{\max}]$ and the beam coverage radius of the UAV is $R_y = h_y \tan \psi_{\rm m}$.

Lemma 1. *In Model 1, the probabilities of the typical user lying in $\mathcal{C}_k, k = 1, 2, 3$, are*

$$A_1^{\rm r} = 1 - e^{-\lambda_{\rm g} \pi D^2}, \quad A_2^{\rm r} < e^{-\lambda_{\rm g} \pi D^2} (1 - e^{-\widetilde{\lambda}_{\rm u} \pi \bar{R}_{\rm r}^2}), \quad A_3^{\rm r} > e^{-\lambda_{\rm g} \pi D^2 - \widetilde{\lambda}_{\rm u} \pi \bar{R}_{\rm r}^2}, \tag{9}$$

TABLE I. Symbols and descriptions. The default values are those used in the numerical results.

Symbol	Description	Default value
$\Phi_{\rm g}$, $\lambda_{\rm g}$	The point process of the GBSs and its density	$\lambda_{\rm g}=1\times10^{-5}$ m^{-2}
$\widetilde{\Phi}_{\rm u}$, $\widetilde{\lambda}_{\rm u}$	The marked point process of the potential UAVs and its density	$\widetilde{\lambda}_{\rm u}=5\times10^{-5}$ m^{-2}
$\Phi_{\rm u}$, $\lambda_{\rm u}$	The marked point process of the UAVs and its density	N/A
$\mu_{\rm g}, \mu_{\rm u}$	The transmit power of the GBS and UAV	$\mu_{\rm g}=40$ W, $\mu_{\rm u}=1$ W
D	The exclusion radius of the GBSs	80 m
$G_{\rm m}, G_{\rm s}, \psi_{\rm m}$	The antenna gains of main lobe and side lobe, and the half HPBW	$10, 1, \frac{\pi}{6}$
$\alpha_{\rm L}, \alpha_{\rm N}$	The path loss exponents for the LOS and NLOS links	$2.5, 4$
$M_{\rm L}, M_{\rm N}$	The fading parameters of the LOS and NLOS links	$4, 1$
ν, κ	The parameters in the LOS probability model	11.95, 0.136 [17]
$h_{\min}, h_{\max}$	The altitude constraints for the UAVs	50 m, 300 m
ζ	The design factor in the dependent-altitude deployment model	10

where $\bar{R}_{\rm r}=(h_{\min}+h_{\max})\tan\psi_{\rm m}/2$ *is the average beam coverage radius for UAVs.*

Proof: Firstly, according to [29, Def. 13.4], $\mathcal{C}_1$ is a Boolean model where the germ point process is a uniform PPP and the grains are the disks with the same deterministic radius D. Hence, using [29, Thm. 13.5] yields $A_1^{\rm r}=\mathbb{P}(o\in\mathcal{C}_1)=1-e^{-\lambda_{\rm g}\pi D^2}$.

Next, with $R_y=h_y\tan\psi_{\rm m}$, $\overline{\mathcal{C}}_2=\bigcup\limits_{(y,h_y)\in\Phi_{\rm u}} b\big(y,R_y\big)$ and $\widetilde{\mathcal{C}}_2=\bigcup\limits_{(y,h_y)\in\widetilde{\Phi}_{\rm u}} b\big(y,R_y\big)$, we have

$$A_2^{\rm r}=\mathbb{P}(o\in\overline{\mathcal{C}}_2, o\notin\mathcal{C}_1)\overset{(a)}{<}\mathbb{P}\big(o\in\widetilde{\mathcal{C}}_2, o\notin\mathcal{C}_1\big)\overset{(b)}{=}(1-e^{-\widetilde{\lambda}_{\rm u}\pi\bar{R}_{\rm r}^2})e^{-\lambda_{\rm g}\pi D^2}, \tag{10}$$

where step (a) follows from $\overline{\mathcal{C}}_2\subset\widetilde{\mathcal{C}}_2$, step (b) follows since $\widetilde{\mathcal{C}}_2$ is a Boolean model where the germ point process is a uniform PPP and the grains are disks with i.i.d. radius, and the final result provides a bound to the association probability $A_2^{\rm r}$.

Finally, the probability of the typical user lying in $\mathcal{C}_3$ is $A_3^{\rm r}=1-A_1^{\rm r}-A_2^{\rm r}$. ■

When $h_{\max}=h_{\min}=h_{\rm f}$, the result in Lemma 1 is reduced to the equal deterministic altitude case.

B. AGIN Model with Location-Dependent Altitudes (Model 2)

In this model, the altitude of each UAV is a function of the horizontal distance to its nearest GBS. As a result, the altitudes of the nearby UAVs are correlated since they may share the same nearest GBS and hence have comparable horizontal distance, which makes the analysis of

the association probability quite challenging. Thus, to facilitate the further analysis, we adopt an *independent-altitude approximation* to decouple the altitudes of different UAVs[2]. Letting $z=\min\limits_{x\in\Phi_{\rm g}}\|y-x\|$ be the horizontal distance from the UAV (y,h_y) to its nearest GBS, the PDF of z is $f_z(v)=2\pi\lambda_{\rm g}ve^{-\pi\lambda_{\rm g}(v^2-D^2)}\mathbf{1}_{v>D}$, from which we can obtain the PDF $f_{h_y}(\nu)$ of its altitude according to (5). Then, the altitude of each UAV is assumed to be independently and identically distributed with $f_{h_y}(\nu)$. From (5), letting $z_{\min}=h^{-1}(h_{\min})$ and $z_{\max}=h^{-1}(h_{\max})$, the average coverage radius of the UAVs according to the total probability law is given by

$$\begin{aligned}\bar{R}_{\rm d}&=\int_D^{\infty}h(v)\tan\psi_{\rm m}f_z(v){\rm d}v\\&=\begin{cases}\Big[h_{\min}\big(1-e^{-\pi\lambda_{\rm g}(z_{\min}^2-D^2)}\big)+h_{\max}e^{-\pi\lambda_{\rm g}(z_{\max}^2-D^2)}+(\frac{\mu_{\rm u}}{\mu_{\rm g}\zeta})^{\frac{1}{\alpha_{\rm L}}}(\pi\lambda_{\rm g})^{\frac{2\alpha_{\rm L}}{\alpha_{\rm N}}}\\\times e^{\pi\lambda_{\rm g}D^2}\Big(\gamma(\frac{\alpha_{\rm N}}{2\alpha_{\rm L}}+1,\pi\lambda_{\rm g}z_{\max}^2)-\gamma(\frac{\alpha_N}{2\alpha_{\rm L}}+1,\pi\lambda_{\rm g}z_{\min}^2)\Big)\Big]\tan\psi_{\rm m} & \text{if } D<z_{\min},\\\Big[(\frac{\mu_{\rm u}}{\mu_{\rm g}\zeta})^{\frac{1}{\alpha_{\rm L}}}(\pi\lambda_{\rm g})^{\frac{2\alpha_{\rm L}}{\alpha_{\rm N}}}e^{\pi\lambda_{\rm g}D^2}\Big(\gamma(\frac{\alpha_{\rm N}}{2\alpha_{\rm L}}+1,\pi\lambda_{\rm g}z_{\max}^2)\\-\gamma(\frac{\alpha_{\rm N}}{2\alpha_{\rm L}}+1,\pi\lambda_{\rm g}z_{\min}^2)\Big)+h_{\max}e^{-\pi\lambda_{\rm g}(z_{\max}^2-D^2)}\Big]\tan\psi_{\rm m} & \text{if } z_{\min}<D<z_{\max},\\\tan\psi_{\rm m}h_{\max}e^{-\pi\lambda_{\rm g}(z_{\max}^2-D^2)} & \text{if } D>z_{\max},\end{cases}\end{aligned}\tag{11}$$

where $\gamma(s,x)=\int_0^x t^{s-1}e^{-t}{\rm d}t$ is the lower incomplete gamma function. Finally, the association probabilities of the typical user are given in the following lemma.

Lemma 2. *In Model 2, the probabilities of the typical user lying in $\mathcal{C}_k, k=1,2,3$, are*

$$A_1^{\rm d}=A_1^{\rm r},\quad A_2^{\rm d}\approx e^{-\lambda_{\rm g}\pi D^2}(1-e^{-\widetilde{\lambda}_{\rm u}\pi\bar{R}_{\rm d}^2}),\quad A_3^{\rm d}\approx e^{-\lambda_{\rm g}\pi D^2-\widetilde{\lambda}_{\rm u}\pi\bar{R}_{\rm d}^2}.\tag{12}$$

Proof: The proof is similar to that of Lemma 1, and the results are approximate due to the independent-altitude approximation. ■

IV. SIR Distribution

In this section, we first give some auxiliary results that are essential for the SIR analysis, including the distance distribution to the serving node and the Laplace transform (LT) of different types of interference, and then provide analytical results on the SIR complementary cumulative distribution functions (CCDFs) of GCUs, GEUs, and UEUs for the two AGIN models.

[2]The independent-altitude approximation can be viewed as a variant of the independent-interferer approximation in [32, 33], which is often adopted to deal with the intractable coupling among different interferers.

A. Model 1

We first analyze the uniformly independent altitude case and then the special case with equal deterministic altitude.

Lemma 3. *For the typical user lying in $\mathcal{C}_1$, the PDF of the horizontal serving distance is*

$$f_1^{\mathrm{r}}(r)=\frac{2\pi\lambda_{\mathrm{g}} r\exp(-\pi\lambda_{\mathrm{g}} r^2)}{1-e^{-\lambda_{\mathrm{g}}\pi D^2}},\quad 0<r\le D. \tag{13}$$

For the typical user lying in $\mathcal{C}_2$, the PDF of the serving UAV's altitude is $\varrho_2^{\mathrm{r}}(u)=\frac{\omega'(u)}{\omega(h_{\max})}$, where

$$\omega(u)=\int_0^{u\tan\psi_{\mathrm{m}}}\frac{u-\varpi(t)}{h_{\max}-h_{\min}}\exp\Big(-2\pi\widetilde{\lambda}_{\mathrm{u}}\int_0^t\frac{h_{\max}-\varpi(v)}{h_{\max}-h_{\min}}v\mathrm{d}v\Big)t\mathrm{d}t, \tag{14}$$

$\omega'(u)$ is the first-order derivative of $\omega(u)$ w.r.t u, and $\varpi(t)=\max(h_{\min},\frac{t}{\tan\psi_{\mathrm{m}}})$. The conditional PDF of the horizontal serving distance is approximated as

$$f_2^{\mathrm{r}}(r\mid h_{y_0}=u)\approx\frac{2\pi\widetilde{\lambda}_{\mathrm{u}} r\exp(-\pi\widetilde{\lambda}_{\mathrm{u}} r^2)}{1-e^{-\widetilde{\lambda}_{\mathrm{u}}\pi u^2\tan^2\psi_{\mathrm{m}}}},\quad 0<r\le u\tan\psi_{\mathrm{m}}. \tag{15}$$

For the typical user lying in $\mathcal{C}_3$, the PDF of the horizontal serving distance $f_3(r)$ is

$$f_3^{\mathrm{r}}(r)\approx\frac{2\pi\lambda_{\mathrm{g}} re^{-\pi\lambda_{\mathrm{g}} r^2+\lambda_{\mathrm{u}}\mathcal{W}(r,D)}}{\int_D^\infty 2\pi\lambda_{\mathrm{g}} te^{-\pi\lambda_{\mathrm{g}} t^2+\lambda_{\mathrm{u}}\mathcal{W}(t,D)}\mathrm{d}t},\quad r>D, \tag{16}$$

where when $h_{\max}\tan\psi_{\mathrm{m}}<2D$,

$$\mathcal{W}(t,D)=\begin{cases}2\int_{t-D}^{h_{\max}\tan\psi_{\mathrm{m}}}\arccos(\frac{v^2+t^2-D^2}{2vt})\frac{h_{\max}-\varpi(v)}{h_{\max}-h_{\min}}v\mathrm{d}v & \text{if } D<t<D+h_{\max}\tan\psi_{\mathrm{m}},\\ 0 & \text{if } t\ge D+h_{\max}\tan\psi_{\mathrm{m}},\end{cases}$$

and when $h_{\max}\tan\psi_{\mathrm{m}}\ge 2D$,

$$\mathcal{W}(t,D)=\begin{cases}2\int_{t-D}^{t+D}\arccos(\frac{v^2+t^2-D^2}{2vt})\frac{h_{\max}-\varpi(v)}{h_{\max}-h_{\min}}v\mathrm{d}v & \text{if } D<t\le h_{\max}\tan\psi_{\mathrm{m}}-D,\\ 2\int_{t-D}^{h_{\max}\tan\psi_{\mathrm{m}}}\arccos(\frac{v^2+t^2-D^2}{2vt})\frac{h_{\max}-\varpi(v)}{h_{\max}-h_{\min}}v\mathrm{d}v & \text{if } |t-h_{\max}\tan\psi_{\mathrm{m}}|\le D,\\ 0 & \text{if } t>D+h_{\max}\tan\psi_{\mathrm{m}}.\end{cases} \tag{17}$$

Proof: See Appendix A.

To reduce the computational complexity of the SIR CCDFs of UEUs and GEUs, we propose two easy-to-compute approximations as follows.

1) UEU: The typical UEU might lie in the vertical coverage regions of several nearby UAVs, and the one with the smallest horizontal distance becomes the serving UAV. Since a UAV with a smaller altitude has a smaller coverage radius, the maximum horizontal distance between a UEU and its potential serving UAV is less than the coverage radius and thus the typical UEU is more likely to associate with the nearby UAV with the smallest altitude. Considering that the altitude of the UAVs has the cumulative distribution function (CDF) $F_{h_y}(u) = \frac{u-h_{\min}}{h_{\max}-h_{\min}}$, $u \in [h_{\min}, h_{\max}]$, and that the serving UAV is chosen from $\vartheta \geq 1$ nearby UAVs on average, we propose an approximation $\widetilde{F}^{\mathrm{r}}(u) = (F_{h_y}(u))^{\vartheta} = \frac{(u-h_{\min})^{\vartheta}}{(h_{\max}-h_{\min})^{\vartheta}}$ for the distribution of the serving UAV's altitude (DSUA) with the approximate PDF $\widetilde{\varrho}_2^{\mathrm{r}}(u) = \mathrm{d}\widetilde{F}^{\mathrm{r}}(u)/\mathrm{d}u$, termed *DSUA approximation*.

2) GEU: For the typical GEU, it is observed from (16) that a term has the Rayleigh distribution form $2\pi\lambda_{\mathrm{g}} r e^{-\pi\lambda_{\mathrm{g}} r^2}$, and the term $\mathcal{W}(r, D)$ yields a higher order power (> 2) in the exponential function. Since the Rayleigh distribution is a special case of the Weibull distribution and a power function is often used to approximate complicated functions, we propose a modified Weibull distribution $\widetilde{f}_3^{\mathrm{r}}(r) = \frac{\chi}{\varsigma}(\frac{r-D}{\varsigma})^{\chi-1} e^{-(\frac{r-D}{\varsigma})^{\chi}} \mathbf{1}_{r>D}$ to approximate $f_3^{\mathrm{r}}(r)$.

The values of ϑ, χ and ς can be obtained by using the **nlinfit** function (nonlinear least-squares fit) in **Matlab** to fit $\varrho_2^{\mathrm{r}}(u)$ and $f_3^{\mathrm{r}}(r)$.

Corollary 1. *When $h_{\max} = h_{\min} = h_{\mathrm{f}}$, the PDFs $f_k^{\mathrm{f}}(r)$ of the horizontal distance between the typical user and its serving node are $f_1^{\mathrm{f}}(r) = f_1^{\mathrm{r}}(r)$, $0 < r \leq D$, and*

$$\begin{aligned} f_2^{\mathrm{f}}(r) &\approx f_2^{\mathrm{r}}(r \mid h_{y_0} = h_{\mathrm{f}}), \quad 0 < r \leq R_{\mathrm{f}}, \\ f_3^{\mathrm{f}}(r) &\approx \frac{2\pi\lambda_{\mathrm{g}} r e^{-\pi\lambda_{\mathrm{g}} r^2 + \lambda_{\mathrm{u}}\xi(R_{\mathrm{f}}, r, D)}}{\int_D^{\infty} 2\pi\lambda_{\mathrm{g}} t e^{-\pi\lambda_{\mathrm{g}} t^2 + \lambda_{\mathrm{u}}\xi(R_{\mathrm{f}}, t, D)} \mathrm{d}t}, \quad r > D, \end{aligned} \tag{18}$$

where $R_{\mathrm{f}} = h_{\mathrm{f}} \tan\psi_{\mathrm{m}}$, and when $R_{\mathrm{f}} < 2D$,

$$\xi(R_{\mathrm{f}}, r, D) = \begin{cases} R_{\mathrm{f}}^2 \arccos(\frac{R_{\mathrm{f}}^2 + r^2 - D^2}{2R_{\mathrm{f}} r}) + D^2 \arccos(\frac{D^2 + r^2 - R_{\mathrm{f}}^2}{2Dr}) \\ \qquad - \frac{1}{2}\sqrt{[(R_{\mathrm{f}} + D)^2 - r^2][r^2 - (R_{\mathrm{f}} - D)^2]} & \text{if } D < r < D + R_{\mathrm{f}}, \\ 0 & \text{if } r > D + R_{\mathrm{f}}, \end{cases}$$

and when $R_{\mathrm{f}} \geq 2D$,

$$\xi(R_{\mathrm{f}}, r, D) = \begin{cases} \pi D^2 & \text{if } D < r < -D + R_{\mathrm{f}}, \\ R_{\mathrm{f}}^2 \arccos(\frac{R_{\mathrm{f}}^2 + r^2 - D^2}{2R_{\mathrm{f}} r}) + D^2 \arccos(\frac{D^2 + r^2 - R_{\mathrm{f}}^2}{2Dr}) & \\ \qquad - \frac{1}{2}\sqrt{[(R_{\mathrm{f}} + D)^2 - r^2][r^2 - (R_{\mathrm{f}} - D)^2]} & \text{if } |r - R_{\mathrm{f}}| < D, \\ 0 & \text{if } r > D + R_{\mathrm{f}}, \end{cases} \tag{19}$$

Proof: The results are directly obtained from Lemma 3.

Next, we focus on the conditional LT of the interference given the serving distance $|x_0| = r$ (or $|y_0| = r$). It should be noted that for the interference analysis, the main technical difficulty lies in the lack of an analytical expression for the probability generating functional (PGFL) of the PHP. As a result, an exact calculation of the LT of the interference from the UAVs seems infeasible and we turn to giving an approximate analytical result by approximating the PHP with a PPP $\Phi_{\rm PPP}$ of density $\lambda_{\rm I}$ outside the exclusion region of the serving GBS[3]. This approach has been used in [34, 35] also.

Theorem 1. *Given the serving distance $|x_0| = r$ (or $|y_0| = r$), the LTs of $I_{\rm g}$ for the typical user lying in $\mathcal{C}_k, k = 1, 2, 3$, are*

$$\mathcal{L}^{\rm r}_{I_{\rm g1}}(s) = \exp\Big(-\frac{2\pi\lambda_{\rm g}\mu_{\rm g} s r^{2-\alpha_{\rm N}}}{\alpha_{\rm N}-2} F(\alpha_{\rm N}, \mu_{\rm g} s r^{-\alpha_{\rm N}})\Big),$$

$$\mathcal{L}^{\rm r}_{I_{\rm g2}}(s) \approx \exp\Big(-\frac{2\pi\lambda_{\rm g}\mu_{\rm g} s D^{2-\alpha_{\rm N}}}{\alpha_{\rm N}-2} F(\alpha_{\rm N}, \mu_{\rm g} s D^{-\alpha_{\rm N}}) + 2\lambda_{\rm g}\int_{r_2}^{D+r} \frac{\arccos\left(\frac{r^2+t^2-D^2}{2rt}\right) t{\rm d}t}{1+(s\mu_{\rm g})^{-1}t^{\alpha_{\rm N}}}\Big), \quad (20)$$

and $\mathcal{L}^{\rm r}_{I_{\rm g3}}(s) = \mathcal{L}^{\rm r}_{I_{\rm g1}}(s)$, where $F(\alpha, y) = {}_2F_1(1, 1-2/\alpha; 2-2/\alpha; -y)$ is the Gaussian hypergeometric function and $r_2 = \max(D, r-D)$, and the LTs of $I_{\rm u}$ are

$$\begin{aligned}
\mathcal{L}^{\rm r}_{I_{\rm u1}}(s) \approx \exp\Bigg(&-2\lambda_{\rm I}\int_{h_{\min}}^{h_{\max}} f(u) \sum_{i\in\{\rm L,N\}} \Bigg(\int_{r_1}^{u\tan\psi_{\rm m}} \pi P_i(t,u)\Psi_i(s,t,u,G_{\rm m}) t{\rm d}t \\
&+ \int_{\bar{r}_1}^{\infty} \pi P_i(t,u)\Psi_i(s,t,u,G_{\rm s}) t{\rm d}t - \int_{r_1}^{\widetilde{r}_1} P_i(t,u)\Psi_i(s,t,u,G_{\rm m}) \arccos\Big(\frac{r^2+t^2-D^2}{2rt}\Big) t{\rm d}t \\
&- \int_{u\tan\psi_{\rm m}}^{\hat{r}_1} P_i(t,u)\Psi_i(s,t,u,G_{\rm s}) \arccos\Big(\frac{r^2+t^2-D^2}{2rt}\Big) t{\rm d}t \Bigg) {\rm d}u \Bigg), \\
\mathcal{L}^{\rm r}_{I_{\rm u2}}(s) \approx \exp\Bigg(&-2\pi\lambda_{\rm I}\int_{h_{\min}}^{h_{\max}} f(u) \sum_{i\in\{\rm L,N\}} \Bigg(\int_{r}^{u\tan\psi_{\rm m}} P_i(t,u)\Psi_i(s,t,u,G_{\rm m}) t{\rm d}t \\
&+ \int_{u\tan\psi_{\rm m}}^{\infty} P_i(t,u)\Psi_i(s,t,u,G_{\rm s}) t{\rm d}t \Bigg) {\rm d}u \Bigg), \\
\mathcal{L}^{\rm r}_{I_{\rm u3}}(s) \approx \exp\Big(&-2\pi\lambda_{\rm I}\int_{h_{\min}}^{h_{\max}} f(u) \sum_{i\in\{\rm L,N\}} \int_{u\tan\psi_{\rm m}}^{\infty} P_i(t,u)\Psi_i(s,t,u,G_{\rm s}) t{\rm d}t{\rm d}u \Big), \qquad (21)
\end{aligned}$$

where $\Psi_i(s,t,u,x) = 1-(1+\frac{s\mu_{\rm u}x}{M_i(t^2+u^2)^{\alpha_i/2}})^{-M_i}$, $r_1 = \min(D-r, u\tan\psi_{\rm m})$, $\bar{r}_1 = \max(D-r, u\tan\psi_{\rm m})$, $\widetilde{r}_1 = \min(D+r, u\tan\psi_{\rm m})$, and $\hat{r}_1 = \max(D+r, u\tan\psi_{\rm m})$.

[3]The approximating PPP is inhomogeneous with constant positive density outside the exclusion region of the serving GBS.

Proof: See Appendix B.

Remark 1. *A natural choice for $\lambda_{\rm I}$ is $\widetilde{\lambda}_{\rm u}$ or $\lambda_{\rm u}$, where $\widetilde{\lambda}_{\rm u}$ yields an upper bound on the interference $I_{\rm u}$ and $\lambda_{\rm u}$ provides an approximation. Since only UAVs outside the exclusion regions are retained, the UAV density in the vicinity of the UEUs is close to $\widetilde{\lambda}_{\rm u}$. Hence, in the integral of (21), using the combination of $\widetilde{\lambda}_{\rm u}$ and $\lambda_{\rm u}$ in the range of $t \in (r, u\tan\psi_{\rm m})$ and $t \in (u\tan\psi_{\rm m}, \infty)$, respectively, would enhance the accuracy.*

When $h_{\max} = h_{\min} = h_{\rm f}$, the conditional LTs of the interference for the three types of users, denoted by $\mathcal{L}^{\rm f}_{I_{\rm g1}}(s)$, $\mathcal{L}^{\rm f}_{I_{\rm g2}}(s)$, and $\mathcal{L}^{\rm f}_{I_{\rm g3}}(s)$, respectively, have the same expressions as in the uniformly independent altitude setting, and those of $I_{\rm u}$ are simplified in the following corollary.

Corollary 2. *When $h_{\max} = h_{\min} = h_{\rm f}$, the LTs of $I_{\rm u}$ given the serving distance $|x_0| = r$ (or $|y_0| = r$) for the typical user lying in $\mathcal{C}_k, k = 1, 2, 3$, are*

$$\begin{aligned}
\mathcal{L}^{\rm f}_{I_{\rm u1}}(s) \approx \exp\Bigg(&- 2\lambda_{\rm I} \sum_{i\in\{\rm L,N\}} \Bigg(\int_{r_1}^{R_{\rm f}} \pi P_i(t,h_{\rm f}) \Psi_i(s,t,h_{\rm f},G_{\rm m}) t {\rm d}t \\
&+ \int_{\bar{r}_1}^{\infty} \pi P_i(t,h_{\rm f}) \Psi_i(s,t,h_{\rm f},G_{\rm s}) t {\rm d}t - \int_{r_1}^{\widetilde{r}_1} P_i(t,h_{\rm f}) \Psi_i(s,t,h_{\rm f},G_{\rm m}) \arccos\Big(\frac{r^2+t^2-D^2}{2rt}\Big) t {\rm d}t \\
&- \int_{R_{\rm f}}^{\hat{r}_1} P_i(t,h_{\rm f}) \Psi_i(s,t,h_{\rm f},G_{\rm s}) \arccos\Big(\frac{r^2+t^2-D^2}{2rt}\Big) t {\rm d}t \Bigg) \Bigg), \\
\mathcal{L}^{\rm f}_{I_{\rm u2}}(s) \approx \exp\Bigg(&- 2\pi\lambda_{\rm I} \sum_{i\in\{\rm L,N\}} \int_{r}^{R_{\rm f}} P_i(t,h_{\rm f}) \Psi_i(s,t,h_{\rm f},G_{\rm m}) t {\rm d}t + \int_{R_{\rm f}}^{\infty} P_i(t,h_{\rm f}) \Psi_i(s,t,h_{\rm f},G_{\rm s}) t {\rm d}t \Bigg), \\
\mathcal{L}^{\rm f}_{I_{\rm u3}}(s) \approx \exp\Bigg(&- 2\pi\lambda_{\rm I} \sum_{i\in\{\rm L,N\}} \int_{R_{\rm f}}^{\infty} P_i(t,h_{\rm f}) \Psi_i(s,t,h_{\rm f},G_{\rm s}) t {\rm d}t \Bigg),
\end{aligned} \tag{22}$$

where $R_{\rm f} = h_{\rm f}\tan\psi_{\rm m}$, $r_1 = \min(D-r, R_{\rm f})$, $\bar{r}_1 = \max(D-r, R_{\rm f})$, $\widetilde{r}_1 = \min(D+r, R_{\rm f})$, and $\hat{r}_1 = \max(D+r, R_{\rm f})$.

Based on the conditional LT of the interference, the SIR CCDF is given in the following.

Theorem 2. *The SIR CCDFs of the typical user lying in $\mathcal{C}_k, k = 1, 2, 3$, are*

$$\begin{aligned}
P^{\rm r}_1(\theta) &\approx \int_0^D \mathcal{L}^{\rm r}_{I_{\rm g1}}(\theta\mu_{\rm g}^{-1} r^{\alpha_{\rm N}}) \mathcal{L}^{\rm r}_{I_{\rm u1}}(\theta\mu_{\rm g}^{-1} r^{\alpha_{\rm N}}) f^{\rm r}_1(r) {\rm d}r, \\
P^{\rm r}_2(\theta) &\approx \int_{h_{\min}}^{h_{\max}} \int_0^{u\tan\psi_{\rm m}} \sum_{i\in\{\rm L,N\}} P_i(r,v) \sum_{l=0}^{M_i-1} \frac{(-s)^l}{l!} \mathcal{L}^{(l)}_2(r,v,s)\big|_{s=\frac{M_i\theta(r^2+v^2)^{\alpha_i/2}}{G_{\rm m}\mu_{\rm u}}} f^{\rm r}_2(r \mid h_{y_0}=v) \varrho^{\rm r}_2(v) {\rm d}r {\rm d}v,
\end{aligned}$$

$$P_3^{\rm r}(\theta) \approx \int_D^{\infty} \mathcal{L}^{\rm r}_{I_{\rm g3}}(\theta\mu_{\rm g}^{-1} r^{\alpha_{\rm N}}) \mathcal{L}^{\rm r}_{I_{\rm u3}}(M_i\theta\mu_{\rm g}^{-1} r^{\alpha_{\rm N}}) f_3^{\rm r}(r){\rm d}r, \tag{23}$$

where $\mathcal{L}_2(r,v,s) = \mathcal{L}^{\rm r}_{I_{\rm g2}}(s)\mathcal{L}^{\rm r}_{I_{\rm u2}}(s)$ is the LT of $I_{\rm g}+I_{\rm u}$ given that the serving UAV is at a distance r and altitude v, and the superscript (l) stands for the l-th derivative of $\mathcal{L}(r,v,s)$ w.r.t. s.

Proof: See Appendix C.

The l-th derivative of $\mathcal{L}(r,v,s)$ can be calculated recursively as shown in the following.

Corollary 3. *Letting*

$$\eta_2(r,v,s) = -2\pi\lambda_{\rm g}\int_D^{\infty} \frac{t{\rm d}t}{1+(s\mu_{\rm g})^{-1}t^{\alpha_{\rm N}}} + 2\lambda_{\rm g}\int_{r_2}^{D+r} \frac{\arccos\left(\frac{r^2+t^2-D^2}{2rt}\right){\rm d}t}{1+(s\mu_{\rm g})^{-1}t^{\alpha_{\rm N}}} - 2\pi\lambda_{\rm I}\int_{h_{\min}}^{h_{\max}} f(u)$$
$$\times \sum_{i\in\{\rm L,N\}} \Big(\int_r^{u\tan\psi_{\rm m}} P_i(t,u)\Psi_i(s,t,u,G_{\rm m})t{\rm d}t + \int_{u\tan\psi_{\rm m}}^{\infty} P_i(t,u)\Psi_i(s,t,u,G_{\rm s})t{\rm d}t\Big){\rm d}u, \tag{24}$$

we have $\mathcal{L}_2(r,v,s) = \exp(\eta_2(r,v,s))$, and $\mathcal{L}^{(l)}(r,v,s)$ is given recursively by

$$\mathcal{L}^{(l)}(r,v,s) = \sum_{n=0}^{l-1} \binom{l-1}{n} \eta_2^{(l-n)}(r,v,s)\mathcal{L}^{(n)}(r,v,s), \tag{25}$$

where the n-th derivative of $\eta_2(r,v,s)$ w.r.t. s is

$$\eta_2^{(n)}(r,v,s) = (-1)^n 2\lambda_{\rm g} n!\Big(\int_D^{\infty} \frac{\pi\mu_{\rm g}^n t^{1-n\alpha_{\rm N}}{\rm d}t}{(1+s\mu_{\rm g}t^{-\alpha_{\rm N}})^{-n-1}} - \int_{r_2}^{D+r} \frac{\mu_{\rm g}^n t^{1-n\alpha_{\rm N}}\arccos\left(\frac{r^2+t^2-D^2}{2rt}\right){\rm d}t}{(1+s\mu_{\rm g}t^{-\alpha_{\rm N}})^{-n-1}}\Big)$$
$$+(-1)^n 2\pi\lambda_{\rm I}\int_{h_{\min}}^{h_{\max}} f(u) \sum_{i\in\{\rm L,N\}} \frac{\Gamma(M_i+n)}{\Gamma(M_i)}\Big(\int_r^{u\tan\psi_{\rm m}} P_i(t,u)\tilde{\Psi}_i(s,t,u,G_{\rm m},n)t{\rm d}t$$
$$+ \int_{u\tan\psi_{\rm m}}^{\infty} P_i(t,u)\tilde{\Psi}_i(s,t,u,G_{\rm s},n)t{\rm d}t\Big){\rm d}u, \tag{26}$$

and $\tilde{\Psi}_i(s,t,u,x,n) = \left(1+\frac{s\mu_{\rm u}x}{M_i(t^2+u^2)^{-\alpha_i/2}}\right)^{-M_i-n}\left(\frac{\mu_{\rm u}x}{M_i(t^2+u^2)^{-\alpha_i/2}}\right)^n$.

Proof: The result is obtained with Thm. 1 for UEUs and the Leibniz formula, similar as in [36, Thm. 2].

Remark 2. *The SIR CCDFs in this general model have four nested integrals, which can be numerically evaluated via jointly using the built-in functions of two **integral2** and one **arrayfun** functions in Matlab 2016 and later versions, but may require extensive computations. To solve this issue, we propose an average-altitude approximation justified by the mean field theory that replaces all interactions with an average or effective interaction. Specifically, the average altitude of the UAVs is substituted into the LTs of the interference in the special case with the equal deterministic altitude, and we adopt these simplified results with three nested integrals to*

approximate the LTs of $I_{\rm u}$. Furthermore, the numerical complexity of the SIR CCDF for UEUs also comes from calculating the derivatives of the LT of the interference, and we use a common upper bound for the incomplete gamma function to obtain a simple approximation to the SIR CCDF in the following corollary.

Corollary 4. *Letting $\beta_i = [\Gamma(M_i+1)]^{-1/M_i}$, a simple approximation on the SIR CCDF of the UEUs is given as*

$$P_2^{\rm r}(\theta) \approx \int_{h_{\min}}^{h_{\max}} \int_0^{u\tan\psi_{\rm m}} \sum_{i\in\{\rm L,N\}} P_i(r,v) \sum_{m=1}^{M_i} \binom{M_i}{m} \mathcal{L}_2(r,v,s)\big|_{s=\frac{m\beta_i M_i \theta (r^2+v^2)^{\alpha_i/2}}{G_{\rm m}\mu_{\rm u}}} f_2^{\rm r}(r \mid h_{y_0}=v) \varrho_2^{\rm r}(v) {\rm d}r{\rm d}v. \tag{27}$$

Proof: Using the inequality $\tilde{\Gamma}(M,x) \le 1-[1-\exp(-\beta x)]^M$ in [37] with $\beta = [\Gamma(M+1)]^{-1/M}$ and $\tilde{\Gamma}(M,x) = \Gamma(M,x)/\Gamma(M)$, a simple approximation can be easily obtained.

Remark 3. *For the special case with equal deterministic altitude, i.e., $h_{\max} = h_{\min} = h_{\rm f}$, the SIR CCDFs can be simplified by removing the expectation over the random UAV altitude, and the expressions of the SIR CCDFs merely have two nested integrals. They can be numerically evaluated efficiently via jointly using the built-in functions of two **integral** and one **arrayfun** functions in Matlab 2016 and later versions, and the infinite upper limits in the multi-level integral sometimes cause a larger numerical error than the predetermined requested accuracy, which can be controlled by replacing the infinite upper limits with an increasing large finite value until the difference between two evaluations with two finite values is less than a predetermined tolerance (say 10^{-5}).*

B. Model 2

In this model, the altitude of each UAV depends on the horizontal distance to its nearest GBS, i.e., both horizontal and vertical dependence are considered. To facilitate the analysis, the independent-altitude approximation and the average-altitude approximation described above are adopted. Letting $\bar{h}_{\rm d} = \bar{R}_{\rm d}/\tan\psi_{\rm m}$ be the average UAV altitude, the PDF $f_k^{\rm d}(r)$ of the horizontal serving distance for the typical user lying in $\mathcal{C}_k, k=1,2,3$, are $f_1^{\rm d}(r) = f_1^{\rm r}(r)$, $0<r\le D$ and

$$\begin{aligned} f_2^{\rm d}(r) &\approx \frac{2\pi\widetilde{\lambda}_{\rm u} r \exp(-\pi\widetilde{\lambda}_{\rm u} r^2)}{1-e^{-\widetilde{\lambda}_{\rm u}\pi\bar{R}_{\rm d}^2}}, \quad 0<r\le \bar{R}_{\rm d}, \\ f_3^{\rm d}(r) &\approx \frac{2\pi\lambda_{\rm g} r e^{-\pi\lambda_{\rm g} r^2 + \lambda_{\rm u}\xi(\bar{R}_{\rm d},r,D)}}{\int_D^\infty 2\pi\lambda_{\rm g} t e^{-\pi\lambda_{\rm g} t^2+\lambda_{\rm u}\xi(\bar{R}_{\rm d},t,D)}{\rm d}t}, \quad r>D. \end{aligned} \tag{28}$$

Since the spatial distributions of the GBSs in the two models are the same, the conditional LTs of $I_{\rm g}$ for the typical user lying in $\mathcal{C}_k, k=1,2,3$, given the serving distance r are the same as in Model 1, i.e., $\mathcal{L}^{\rm d}_{I_{\rm g1}}(s)=\mathcal{L}^{\rm r}_{I_{\rm g1}}(s)$, $\mathcal{L}^{\rm d}_{I_{\rm g2}}(s)=\mathcal{L}^{\rm r}_{I_{\rm g2}}(s)$, and $\mathcal{L}^{\rm d}_{I_{\rm g3}}(s)=\mathcal{L}^{\rm r}_{I_{\rm g3}}(s)$. Furthermore, the LTs of $I_{\rm u}$ for three types of users are obtained via replacing $h_{\rm f}$ and $R_{\rm f}$ with $\bar{h}_{\rm d}$ and $\bar{R}_{\rm d}$ in the corresponding expressions in Corollary 2, respectively.

Finally, the SIR CCDFs of the typical user lying in $\mathcal{C}_k, k=1,2,3$, are

$$\begin{aligned}
P^{\rm d}_1(\theta)&\approx\int_0^{D}\mathcal{L}^{\rm d}_{I_{\rm g1}}(\theta\mu_{\rm g}^{-1}r^{\alpha_{\rm N}})\mathcal{L}^{\rm d}_{I_{\rm u1}}(\theta\mu_{\rm g}^{-1}r^{\alpha_{\rm N}})f^{\rm d}_1(r){\rm d}r,\\
P^{\rm d}_2(\theta)&\approx\sum_{i\in\{\rm L,N\}}\int_0^{\bar{R}_{\rm d}}P_i(r,\bar{h}_{\rm d})\sum_{l=0}^{M_i-1}\frac{(-s)^l}{l!}\mathcal{L}^{(l)}_2(r,\bar{h}_{\rm d},s)\big|_{s=\frac{M_i\theta(r^2+\bar{h}_{\rm d}^2)^{\alpha_i/2}}{G_{\rm m}\mu_{\rm u}}}f^{\rm d}_2(r){\rm d}r\\
&\approx\sum_{i\in\{\rm L,N\}}\int_0^{\bar{R}_{\rm d}}P_i(r,\bar{h}_{\rm d})\sum_{m=1}^{M_i}\binom{M_i}{m}\mathcal{L}_2(r,\bar{h}_{\rm d},,s)\big|_{s=\frac{m\beta_iM_i\theta(r^2+\bar{h}_{\rm d}^2)^{\alpha_i/2}}{G_{\rm m}\mu_{\rm u}}}f^{\rm d}_2(r){\rm d}r,\\
P^{\rm d}_3(\theta)&\approx\int_D^{\infty}\mathcal{L}^{\rm d}_{I_{\rm g3}}(\theta\mu_{\rm g}^{-1}r^{\alpha_{\rm N}})\mathcal{L}^{\rm d}_{I_{\rm u3}}(\theta\mu_{\rm g}^{-1}r^{\alpha_{\rm N}})f^{\rm d}_3(r){\rm d}r,
\end{aligned}\tag{29}$$

where $\mathcal{L}_2(r,\bar{h}_{\rm d},s)=\mathcal{L}^{\rm d}_{I_{\rm g2}}(s)\mathcal{L}^{\rm d}_{I_{\rm u2}}(s)$.

C. Overall Performance

According to the association probabilities of the typical user lying in different regions and their corresponding SIR CCDFs, the overall SIR distribution of the typical user is

$$P(\theta)=\sum_{k=1,2,3}A_kP_k(\theta).\tag{30}$$

In addition to the SIR distribution which characterizes the link-level performance, it is necessary to investigate the area spectral efficiency, which characterizes the network-level performance. Since the users lying in $\mathcal{C}_1$ and $\mathcal{C}_3$ are served by GBSs, the overall SIR distribution of GBSs is

$$P_{\rm g}(\theta)=\frac{A_1P_1(\theta)+A_3P_3(\theta)}{A_1+A_3}.\tag{31}$$

Hence, under the fixed-rate transmission, each UAV provides the spectral efficiency by $P_2(\theta)\log_2(1+\theta)$ and each GBS provides the spectral efficiency by $P_{\rm g}(\theta)\log_2(1+\theta)$, and then the area spectral efficiency (ASE) is obtained via multiplying the corresponding densities of UAVs and GBSs, respectively, which can be expressed by

$${\rm ASE}=\big(\lambda_{\rm g}P_{\rm g}(\theta)+\lambda_{\rm u}P_2(\theta)\big)\log_2(1+\theta).\tag{32}$$

V. NUMERICAL RESULTS

In this section, we present numerical results of the performance evaluation in different UAV deployment strategies, and simulation results are also provided to validate the approximations. The simulation region is $[0, 20000]^2$, and the horizontal locations of the GBSs and potential UAVs are first generated via following the homogeneous PPP realization. Then, the horizontal distance of each potential UAV to its closest GBS is calculated to determine whether it is retained according to the exclusion radius, and the altitudes of UAVs are generated according to the two models. For each network realization, the locations of 10000 users are generated following the random and uniform distribution in the simulation region, and the association procedure is performed on each user to determine its serving access point, i.e., the user type is determined. This way, the simulation results for the association probabilities and the empirical distribution of the serving distances for the three user types can be obtained. The received SIR is further calculated via independently generating gamma-distributed random variables as the small-scaling power coefficients and determining the antenna gain from the UAV to the user after determining whether the user lies in the vertical coverage region of the UAV. This process is repeated until the number of the GCU samples, GEU samples, and UEU samples all reach 100000, and then the empirical distributions of the SIRs for the three user types are obtained. To avoid the boundary effect, we focus on the users located in the central square of $[5000, 15000]^2$. The default values of the parameters are given in Table I where applicable.

Figs. 2 and 3 show how the density of the potential UAVs $\widetilde{\lambda}_{\mathrm{u}}$ and the exclusion radius of GBSs D affect the association probabilities of the typical user lying in different regions (or being a GCU, GEU, or UEU), where a special case of Model 1 with $h_{\max} = h_{\min} = h_{\mathrm{f}} = 175$ is also considered. It can be seen that the analytical results match the simulations well, validating the accuracy of the approximations. The association probabilities in Model 1 are the same for equal deterministic altitude and uniformly independent altitude settings because the coverage radius of UAVs with equal deterministic altitude $h_{\mathrm{f}} = 175$ is equal to the average coverage radius in the uniformly independent altitude model under the current parameter settings. From both figures, we can observe that the density and altitude of UAVs as well as the exclusion radius are key parameters that can be used to balance the load between the GBSs and UAVs flexibly. In particular, more edge users can be assigned to the UAVs with location-dependent altitudes to get better performance than from the GBSs.

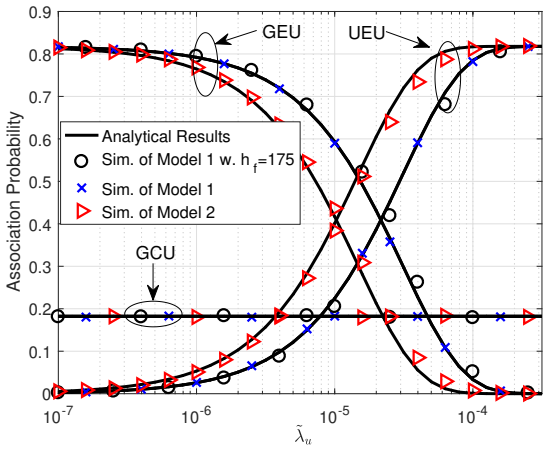

Fig. 2. The association probability of the typical user versus the density of potential UAVs with $D = 80\mathrm{m}$.

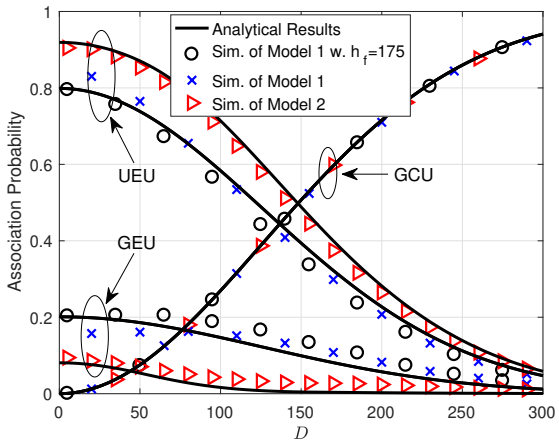

Fig. 3. The association probability of the typical user versus the exclusion radius of GBSs.

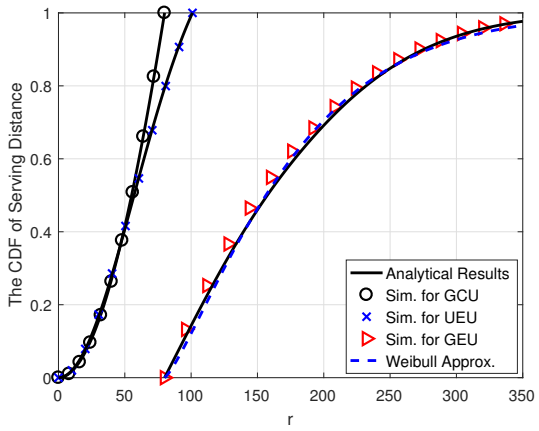

(a) Model 1 with equal deterministic altitude.

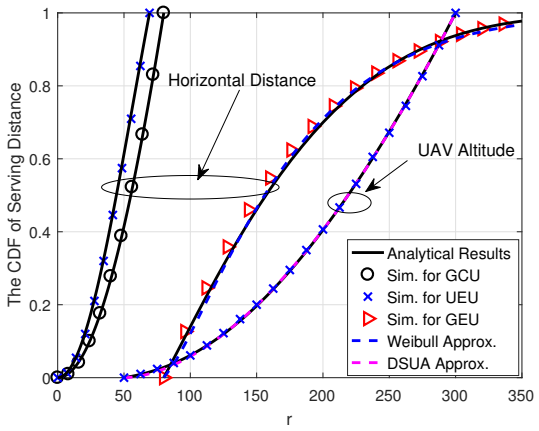

(b) Model 1 with uniformly independent altitude.

Fig. 4. The validation of the approximations for the distance distributions for Model 1.

Fig. 4 validates the approximation on the horizontal and vertical serving distance distributions in both equal deterministic- and uniformly independent-altitude models, where the conditional horizontal serving distance of the UEU is obtained given that $h_{y_0} = 120$. It can be seen that the analytical results of both distances match well with their simulations. The proposed Weibull distribution provides an excellent approximation to the horizontal serving distance distribution for GUEs in both cases, and the proposed DSUA approximation is quite close to the distribution of the serving UAV's altitude in the uniformly independent altitude model.

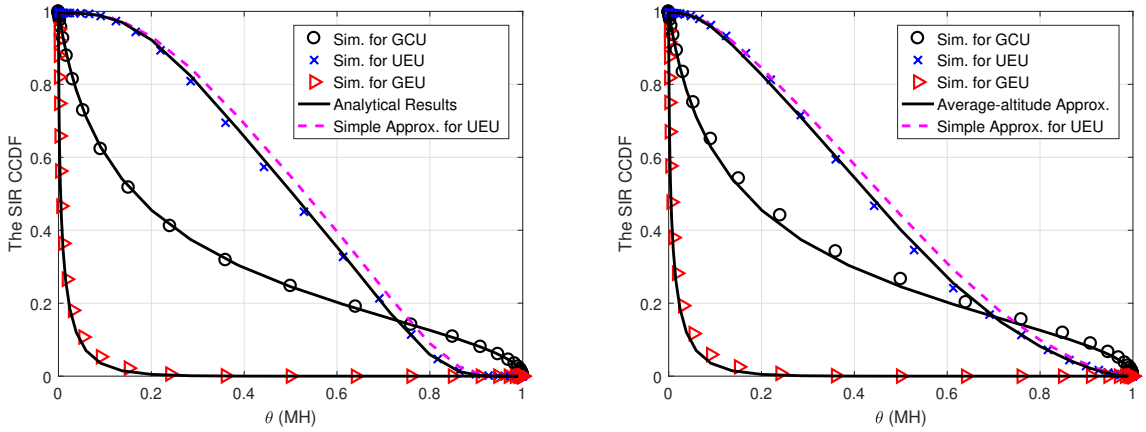

(a) Model 1 with equal deterministic altitude.

(b) Model 1 with uniformly independent altitude.

Fig. 5. The validation of the approximations for the SIR CCDFs of GCUs, UEUs and GEUs for Model 1.

Since the SIR threshold in linear unit is $\theta \in \mathbb{R}^+$ (or $\theta \in \mathbb{R}$ in dB form), a plot showing the SIR distribution as a function of θ or θ in dB cannot reveal the complete information. Hence, we plot it in *Möbius homeomorphic* (MH) units, via the transformation $\theta\,(\mathrm{MH}) = \theta/(1+\theta)$, resulting in $\theta\,(\mathrm{MH}) \in [0,\ 1]$ [38] in Fig. 5. It can be seen that the analytical results on the SIR distributions match well with their simulations. The proposed average-altitude approximation performs well in calculating the SIR CCDFs for GCUs, UEUs and GEUs, exhibiting its high efficiency in reducing the computational complexity without sacrificing the accuracy. The simple approximation using the inequality of incomplete gamma function on the UEU SIR distribution are also close to the simulations, which further improves the computational efficiency in the scenarios with Nakagami fading. To quantify the match level of the approximate results, we use the MH distance [27], defined as $d_{\mathrm{MH}}(F,G) \triangleq \int_0^1 |F(t)-G(t)|\mathrm{d}t$, where $F(t)$ is the curve in MH units based on simulation data serving as the ground truth and $G(t)$ is the analytical curve in the MH unit. The MH distance is bounded by 1 and the specific value directly and unambiguously measures the match between the analytical approximation and simulation results on the SIR distributions. As in [27], we also use the six match levels "bad", "mediocre", "acceptable", "good, "excellent, "perfect" corresponding to the MH distance ranges 0.05-1, 0.02-0.05, 0.01-0.02, 0.005-0.01, 0.002-0.005, 0-0.002, respectively. The final results are shown in Table II for the three types of users in different models. In addition, we observe that the SIR performance of UEUs in Model 1 with uniformly independent altitude is slightly worse than that in Model 1 with

TABLE II. The MH distance and match level of the analytical approximations.

	Equal deterministic altitude model		Uniformly independent altitude model		Model 2	
	MH Distance	Match Level	MH Distance	Match Level	MH Distance	Match Level
GCU	0.0021	Excellent	0.0166	Acceptable	0.0078	Good
GEU	0.0034	Excellent	0.0048	Excellent	9.4×10^{-4}	Perfect
UEU	0.0070	Good	0.0074	Good	0.0269	Mediocre
Simple Approx.	0.0288	Mediocre	0.0242	Mediocre	0.0372	Mediocre

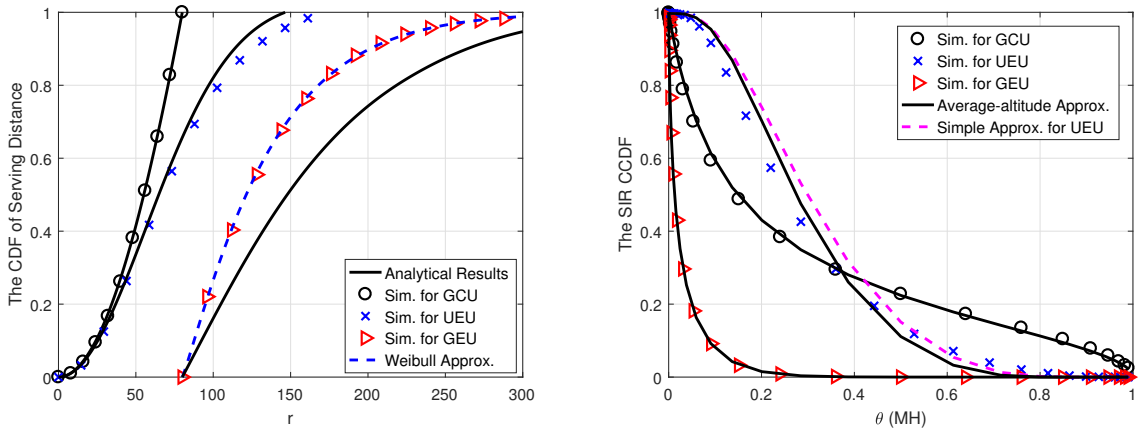

(a) The distribution of the horizontal serving distance.

(b) The SIR CCDFs of GCUs, UEUs and GEUs.

Fig. 6. The validation of the approximations for Model 2.

equal deterministic altitude under the same parameter settings. This implies that random altitudes increase the uncertainty of the quality of service from UAVs but would be more realistic.

Fig. 6 validates the approximations concerning the serving distance and SIR distributions in Model 2, where the SIR distributions are also plotted in the MH unit in Fig. 6(b) with the MH distance and match level for each type of user shown in Table II. Due to the adoption of the average-altitude approximation, the analytical serving distance distribution of GEUs shows an obvious deviation from the simulation. But the proposed Weibull distribution provides a rather close approximation, making up for this deviation and ensuring the accuracy of the further analytical results on the SIR distribution. Compared with Fig. 5, it is found that although the SIR performance improvement of the UEUs in Model 2 is not as large as in Model 1, the fraction of the GEUs is significantly decreased from 0.1645 in Model 1 to 0.0281 in Model

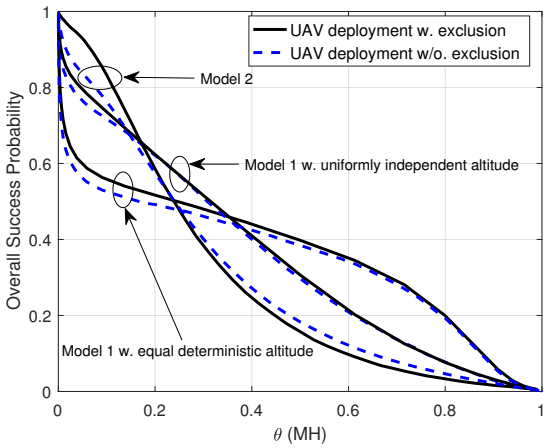

Fig. 7. The overall SIR distribution of the typical user.

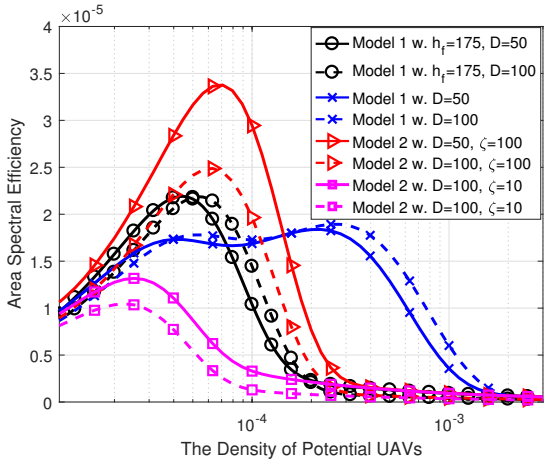

Fig. 8. The ASE versus the density of potential UAVs.

2, i.e., dropping about sixfold, seen from Fig. 3 with $D = 80\,\mathrm{m}$. This reveals an important trade-off between the link and network performance in terms of the UAV's altitude. Specifically, the UAV's altitude determines its beam coverage and the received signal strength at the served users. The beam coverage increases with the UAV's altitude, leading to more edge users to be served by UAVs rather than GBSs. At the same time, however, the desired signal strength of the UEUs decreases with the increase of the altitude due to the propagation loss. Thus, to fully study the intricate relations, we further analyze the overall performance of AGINs next.

Fig. 7 shows the overall SIR distributions for the two models with $\widetilde{\lambda}_{\mathrm{u}} = 2\lambda_{\mathrm{g}}$ and $h_{\mathrm{f}} = 120\,\mathrm{m}$, comparing with the case without exclusion regions of GBSs obtained through simulations, where the distribution of UAVs follows a marked PPP with the same density $\lambda_{\mathrm{u}} = \widetilde{\lambda}_{\mathrm{u}} e^{-\lambda_{\mathrm{g}}\pi D^2}$. It can be seen that the proposed AGIN model with exclusion regions yields a better overall performance than the case without exclusion regions in ranges with low SIR (e.g., $\theta < 0.25\,\mathrm{MH} \approx -5\,\mathrm{dB}$) and a comparable performance for other ranges (e.g., $\theta > 0.25\,\mathrm{MH} \approx -5\,\mathrm{dB}$). This corroborates the necessity of using an exclusion region when deploying the UAVs in AGINs, which effectively reduces the mutual interference and improves the edge user's performance. Furthermore, Model 2 performs the best in serving the users with a relatively low SIR which are likely to be located near the cell edge. Since the location-dependent UAV deployment provides a flexible beam coverage that closely tracks the locations of users and their received signal strength from the nearest GBSs, it allows more edge users to access the UAVs and effectively improves their

performance, thus driving the improvement of the overall performance. This shows that Model 2 is suitable for scenarios with low rate but massive connectivity requirements.

Fig. 8 investigates the influence of the potential UAV density on the ASE for the two models with $\theta = 0$ dB. It is observed that the ASEs first increase and then decrease after reaching the maximum point with $\widetilde{\lambda}_{\mathrm{u}}$ in the cases of Model 1 with equal deterministic altitude and Model 2, while Model 1 with uniformly independent altitude yields a slightly different trend in the range of $\widetilde{\lambda}_{\mathrm{u}} \in [4\times10^{-5}, 3\times10^{-4}]$. Increasing $\widetilde{\lambda}_{\mathrm{u}}$ means to deploy more UAVs to assist GBSs enhancing the performance of more edge users, which, however, exacerbates the mutual interference and hence decreases the link transmission reliability. The competing effects on the ASE lead to the varying trend of the three curves. Furthermore, Model 2 with $D = 50\,\mathrm{m}$ and $\zeta = 100$ performs best in the sparse UAV deployment ($\widetilde{\lambda}_{\mathrm{u}} < 1.5 \times 10^{-4}\,\mathrm{m}^{-2}$) since it provides the best coverage given the current parameter setting, while the case with $\zeta = 10$ leads to the worst performance. This shows that the key parameter ζ should be judiciously chosen to show the advantage of the location-dependent UAV deployment scheme. When $\widetilde{\lambda}_{\mathrm{u}} > 1.5 \times 10^{-4}\,\mathrm{m}^{-2}$, Model 1 with uniformly independent altitude provides the best ASE, because the UAVs may hover at a low altitude, providing a small beam coverage and causing less interference to other concurrent links. Hence this deployment can tolerate more UAVs coexisting in the AGINs.

VI. Conclusion

In this paper, we propose two new AGIN models to capture the spatial dependence present in real deployments. The horizontal dependence is modeled by an exclusion region of each GBS such that UAVs can only be deployed outside, and the vertical dependence is reflected by the varied altitude settings of the UAVs. The locations of GBSs and UAVs are modeled as a PPP and a MPHP, respectively, where the marks in the MPHP correspond to the UAVs' altitude. Each UAV is equipped with a directional antenna array to provide a downward beam coverage flexibly adapted to the UAV's altitude and the beamwidth of the main lobe. In stark contrast, existing works disregarded the coverage by the UAVs or assumed a fixed coverage region independent of the other network parameters. Using the tools from stochastic geometry, we provide analytical results for each model, including the association probability, horizontal distance distributions, altitude distributions, SIR distribution as well as area spectral efficiency. The adoptions of a

modified Weibull distribution and an approximate distribution for the serving UAV's altitude in the analysis help simplify the results significantly, without affecting their accuracy.

The results expose two key insights: 1) there is a trade-off between the link-level and network-level performance regarding to the UAV deployment, i.e., increasing the UAV's altitude expands its beam coverage but weakens the desired signal strength of the served user at the same time; 2) it is necessary to propose and study AGIN models with spatial dependence between the aerial and terrestrial network layers; the results obtained based on such models can in turn more sensibly guide the deployment of actual networks than the current independent models.

APPENDIX A
PROOF OF LEMMA 3

For the typical user lying in $\mathcal{C}_1$, the CDF of the serving distance $\|x_0\|$ is

$$F_1(r) = \mathbb{P}(\|x_0\| \le r \mid \|x_0\| \le D) = \frac{1-e^{-\lambda_{\rm g}\pi r^2}}{1-e^{-\lambda_{\rm g}\pi D^2}}, \quad 0 < r \le D. \tag{33}$$

Next, for the typical user lying in $\mathcal{C}_2$, both the altitude and horizontal distance of the serving UAV are random variables due to the uniformly independent altitude deployment. Thus, we first derive the altitude distribution and then give the conditional distribution of the horizontal distance given the altitude. Letting (y_0, h_{y_0}) be the serving UAV and

$$\mathcal{E}(u,\Phi_{\rm u}) \triangleq \sum_{(y_0,h_{y_0})\in\Phi_{\rm u}} \mathbf{1}_{\|y_0\|\le h_{y_0}\tan\psi_{\rm m}, h_{y_0}\le u} \prod_{(y,h_y)\in\Phi_{\rm u}^{!}} \left(\mathbf{1}_{\|y\|>\|y_0\|} + \mathbf{1}_{h_y\tan\psi_{\rm m}<\|y\|\le\|y_0\|}\right), \tag{34}$$

we have $\mathcal{E}(u,\Phi_{\rm u}) \in \{1,0\}$, where $\mathcal{E}(u,\Phi_{\rm u}) = 1$ is the event that the typical user lies in the coverage region of the UAV (y_0, h_{y_0}) and $h_{y_0} \le u$, and vice versa. Then we have

$$\begin{aligned} F^{\rm r}_{h_{y_0}}(u) &= \frac{\mathbb{P}(h_{y_0}\le u, \min\limits_{x\in\Phi_{\rm g}}\|x\| > D, \mathcal{E}(h_{\max},\Phi_{\rm u})=1)}{\mathbb{P}(\min\limits_{x\in\Phi_{\rm g}}\|x\| > D, \mathcal{E}(h_{\max},\Phi_{\rm u})=1)} \\ &= \frac{\mathbb{P}(\mathcal{E}(u,\Phi_{\rm u})=1, \min\limits_{x\in\Phi_{\rm g}}\|x\| > D)}{\mathbb{P}(\min\limits_{x\in\Phi_{\rm g}}\|x\| > D, \mathcal{E}(h_{\max},\Phi_{\rm u})=1)} \\ &\overset{(a)}{\approx} \frac{\mathbb{P}(\mathcal{E}(u,\widetilde{\Phi}_{\rm u})=1)}{\mathbb{P}(\mathcal{E}(h_{\max},\widetilde{\Phi}_{\rm u})=1)} = \frac{\mathbb{E}(\mathcal{E}(u,\widetilde{\Phi}_{\rm u}))}{\mathbb{E}(\mathcal{E}(h_{\max},\widetilde{\Phi}_{\rm u}))}, \quad h_{\min}\le u\le h_{\max}, \end{aligned} \tag{35}$$

where step (a) follows the fact that the nearest horizontal distance to the points in $\widetilde{\Phi}_{\rm u}$ is smaller than that in $\Phi_{\rm u} \subset \widetilde{\Phi}_{\rm u}$ and the independence between $\Phi_{\rm g}$ and $\widetilde{\Phi}_{\rm u}$. According to the Campbell-Mecke theorem [29, Thm. 8.2], we have

$$\begin{aligned}\mathbb{E}[\mathcal{E}(u,\widetilde{\Phi}_{\rm u})] &= \widetilde{\lambda}_{\rm u}\int_{\mathbb{R}^2}\mathbb{E}\Big[\mathbf{1}_{\|y_0\|\le h_{y_0}\tan\psi_{\rm m},h_{y_0}\le u}\prod_{(y,h_y)\in\tilde{\Phi}_{\rm u}^{!}}\big(\mathbf{1}_{\|y\|>\|y_0\|}+\mathbf{1}_{h_y\tan\psi_{\rm m}<\|y\|\le\|y_0\|}\big)\Big]{\rm d}y_0\\ &= 2\pi\widetilde{\lambda}_{\rm u}\int_0^{u\tan\psi_{\rm m}}\frac{u-\varpi(t)}{h_{\max}-h_{\min}}\exp\Big(-2\pi\widetilde{\lambda}_{\rm u}\int_0^t(1-\mathbb{E}\mathbf{1}_{h_y\tan\psi_{\rm m}<v})v{\rm d}v\Big)t{\rm d}t\\ &= 2\pi\widetilde{\lambda}_{\rm u}\int_0^{u\tan\psi_{\rm m}}\frac{u-\varpi(t)}{h_{\max}-h_{\min}}\exp\Big(-2\pi\widetilde{\lambda}_{\rm u}\int_0^t\frac{h_{\max}-\varpi(v)}{h_{\max}-h_{\min}}v{\rm d}v\Big)t{\rm d}t, \end{aligned}\tag{36}$$

and $\mathbb{E}[\mathcal{E}(h_{\max},\widetilde{\Phi}_{\rm u})]$ can be derived similarly.

Given the serving altitude u, the CDF of the serving horizontal distance $\|y_0\|$ is

$$\begin{aligned}F_2(r) &= \mathbb{P}(\|y_0\|\le r \mid \min_{x\in\Phi_{\rm g}}\|x\|>D, \|y_0\|\le u\tan\psi_{\rm m})\\ &= \frac{\mathbb{P}(\|y_0\|\le r, \min_{x\in\Phi_{\rm g}}\|x\|>D)}{\mathbb{P}(\min_{x\in\Phi_{\rm g}}\|x\|>D, \|y_0\|\le u\tan\psi_{\rm m})} \overset{(b)}{\approx} \frac{1-e^{-\widetilde{\lambda}_{\rm u}\pi r^2}}{1-e^{-\widetilde{\lambda}_{\rm u}\pi u^2\tan^2\psi_{\rm m}}}, \quad 0<r\le u\tan\psi_{\rm m}, \end{aligned}\tag{37}$$

where step (b) follows the same fact as in step (a).

Finally, for the typical GUE, letting x_0 be the serving GBS and $\widetilde{\mathcal{E}}(\Phi_{\rm u}) \triangleq \prod_{(y,h_y)\in\Phi_{\rm u}}\mathbf{1}_{h_y\tan\psi_{\rm m}<\|y\|}$, the CDF of the serving distance $\|x_0\|$ is

$$F_3(r) = \frac{\mathbb{P}(\|x_0\|\le r, \|x_0\|>D, \widetilde{\mathcal{E}}(\Phi_{\rm u})=1)}{\mathbb{P}(\|x_0\|>D, \widetilde{\mathcal{E}}(\Phi_{\rm u})=1)}.\tag{38}$$

We further obtain that

$$\begin{aligned}\mathbb{P}(\|x_0\|>D, \widetilde{\mathcal{E}}(\Phi_{\rm u})=1) &= \int_D^\infty f_{\|x_0\|}(t)\mathbb{E}\big[\widetilde{\mathcal{E}}(\Phi_{\rm u})\big]{\rm d}t\\ &\approx \int_D^\infty f_{\|x_0\|}(t)\exp\Big(-\lambda_{\rm u}\underbrace{\int_{\mathbb{R}^2\setminus b(x_0,D)}1-\mathbb{E}\mathbf{1}_{h_y\tan\psi_{\rm m}<\|y\|}{\rm d}y}_{\widetilde{\mathcal{W}}(t,D)}\Big){\rm d}t, \end{aligned}\tag{39}$$

where $f_{\|x_0\|}(t) = 2\pi\lambda_{\rm g}te^{-\pi\lambda_{\rm g}t^2}$ is the serving distance PDF of the typical user, and $\widetilde{\mathcal{W}}(t,D)$ can be obtained with the integral technique and the geometry relationship of two circles. Similarly, we obtain the numerator of (38) and thus the PDF $f_3^{\rm r}(r)$, and $\mathcal{W}(t,D)$ in Lemma 3 is further obtained by removing a common factor in both numerator and denominator of (38), given by

$$\mathcal{W}(t,D) = \widetilde{\mathcal{W}}(t,D) - 2\pi\int_0^{h_{\max}\tan\psi_{\rm m}}\frac{h_{\max}-\varpi(v)}{h_{\max}-h_{\min}}v{\rm d}v.\tag{40}$$

APPENDIX B
PROOF OF THEOREM 1

Given that the serving distance is r, we derive the conditional LTs of the interference $I_{\rm g}$ and $I_{\rm u}$ for each type of the user.

Firstly, for the typical user lying in $\mathcal{C}_1$, we have $r < D$ and the LT of $I_{\rm g}$

$$\begin{aligned}\mathcal{L}^{\rm r}_{I_{\rm g1}}(s) &\overset{(a)}{=} \mathbb{E}\Big[\prod_{x\in\Phi^{\rm l}_{\rm g}} \frac{1}{1+s\mu_{\rm g}\ell_{\rm g}(x)}\Big]\\ &\overset{(b)}{=} \exp\Big(-2\pi\lambda_{\rm g}\int_r^{\infty}\Big(1-\frac{1}{1+s\mu_{\rm g}\ell_{\rm g}(t)}\Big)t{\rm d}t\Big)\\ &= \exp\Big(-\frac{2\pi\lambda_{\rm g}\mu_{\rm g}sr^{2-\alpha_{\rm N}}}{\alpha_{\rm N}-2}F(\alpha_{\rm N},\mu_{\rm m}sr^{-\alpha_{\rm N}})\Big),\end{aligned} \tag{41}$$

where step (a) uses the exponential distribution of the power fading coefficient for NLOS links, step (b) follows the PGFL of a PPP, and $F(\alpha,y) = {}_2F_1(1,1-2/\alpha;2-2/\alpha;-y)$ is the Gaussian hypergeometric function. For the LT of $I_{\rm u}$, it is difficult to exactly characterize the interference from the UAVs due to the complexity of the PHP. Instead, we resort to approximating the PHP with a PPP of density $\lambda_{\rm I}$ and removing the UAVs in the exclusion region of the serving GBS [34, 35]. Thus, the approximate LT of $I_{\rm u}$ is given by

$$\begin{aligned}\mathcal{L}^{\rm r}_{I_{\rm u1}}(s) &\overset{(c)}{=} \mathbb{E}\Big[\prod_{(y,h_y)\in\Phi_{\rm u}}\sum_{i\in\{\rm L,N\}}\frac{P_i(\|y\|,h_y)}{\big(1+\frac{sG(\phi_y)\mu_{\rm u}}{M_i}(\|y\|^2+h_{\rm f}^2)^{-\alpha_i/2}\big)^{M_i}}\Big]\\ &\overset{(d)}{\approx} \mathbb{E}\Big[\prod_{y\in\Phi_{\rm PPP}\setminus\xi_{\rm ex}}\sum_{i\in\{\rm L,N\}}\frac{P_i(\|y\|,h_y)}{\big(1+\frac{sG(\phi_y)\mu_{\rm u}}{M_i}(\|y\|^2+h_y^2)^{-\alpha_i/2}\big)^{M_i}}\Big]\\ &= \exp\Bigg(-2\pi\lambda_{\rm I}\sum_{i\in\{\rm L,N\}}\int_{h_{\min}}^{h_{\max}}f(u)P_i(t,u)\Bigg(\int_{r_1}^{u\tan\psi_{\rm m}}\Big(1-\frac{1}{(1+\frac{s\mu_{\rm u}G_{\rm m}}{M_i(t^2+u^2)^{\alpha_i/2}})^{M_i}}\Big)t{\rm d}t\\ &\quad+\int_{\bar r_1}^{\infty}\Big(1-\frac{1}{(1+\frac{s\mu_{\rm u}G_{\rm s}}{M_i(t^2+u^2)^{\alpha_i/2}})^{M_i}}\Big)t{\rm d}t-\int_{r_1}^{\widetilde r_1}\Big(1-\frac{1}{(1+\frac{s\mu_{\rm u}G_{\rm m}}{M_i(t^2+u^2)^{\alpha_i/2}})^{M_i}}\Big)\arccos(\frac{r^2+t^2-D^2}{2rt})t{\rm d}t\\ &\quad-\int_{u\tan\psi_{\rm m}}^{\hat r_1}\Big(1-\frac{1}{(1+\frac{s\mu_{\rm u}G_{\rm s}}{M_i(t^2+u^2)^{\alpha_i/2}})^{M_i}}\Big)\arccos(\frac{r^2+t^2-D^2}{2rt})t{\rm d}t\Bigg){\rm d}u\Bigg).\end{aligned} \tag{42}$$

In step (c), the power fading coefficients follow the gamma and exponential distributions for NLOS and LOS links, respectively, and in step (d), the PPP $\Phi_{\rm PPP}$ is adopted to approximate the PHP and $\xi_{\rm ex} = b(x_0, D)$ denotes the exclusion region of the serving GBS x_0. The last step follows that the antenna gain from an interfering UAV is $G_{\rm m}$ if the horizontal distance is shorter than $R_y = u\tan\psi_{\rm m}$, otherwise, the gain is $G_{\rm s}$.

Secondly, when the typical user is a UEU, we obtain the LT of $I_{\rm g}$, given by

$$\begin{aligned}\mathcal{L}^{\rm r}_{I_{\rm g2}}(s)&=\mathbb{E}\Big[\prod_{x\in\Phi_{\rm g}}\frac{1}{1+s\mu_{\rm g}\ell_{\rm g}(x)}\Big]\\&=\exp\bigg(-\lambda_{\rm g}\int_{\mathbb{R}^2\setminus b(o,D)}\frac{1}{1+(s\mu_{\rm g})^{-1}\|x\|^{\alpha_{\rm N}}}{\rm d}x+\lambda_{\rm g}\int_{\xi_{\rm ex}\setminus b(o,D)}\frac{1}{1+(s\mu_{\rm g})^{-1}\|x\|^{\alpha_{\rm N}}}{\rm d}x\bigg)\\&=\exp\bigg(-\frac{2\pi\lambda_{\rm g}\mu_{\rm g}sD^{2-\alpha_{\rm N}}}{\alpha_{\rm N}-2}F(\alpha_{\rm N},\mu_{\rm m}sD^{-\alpha_{\rm N}})+\lambda_{\rm g}\int_{\xi_{\rm ex}\setminus b(o,D)}\frac{1}{1+(s\mu_{\rm g})^{-1}\|x\|^{\alpha_{\rm N}}}{\rm d}x)\bigg),\end{aligned}\tag{43}$$

where $\xi_{\rm ex}=b(y_0,D)\cup b(o,D)$ denotes the region without GBSs. We further have

$$\int_{\xi_{\rm ex}\setminus b(o,D)}\frac{1}{1+(s\mu_{\rm g})^{-1}\|x\|^{\alpha_{\rm N}}}{\rm d}x=\begin{cases}\int_{D}^{D+r}\frac{\arccos\left(\frac{r^2+t^2-D^2}{2rt}\right)t{\rm d}t}{1+(s\mu_{\rm g})^{-1}t^{\alpha_{\rm N}}} & \text{if } r<2D,\\ \int_{r-D}^{D+r}\frac{\arccos\left(\frac{r^2+t^2-D^2}{2rt}\right)t{\rm d}t}{1+(s\mu_{\rm g})^{-1}t^{\alpha_{\rm N}}} & \text{if } r>2D.\end{cases}\tag{44}$$

Combining the two cases, we obtain the unified expression

$$\mathcal{L}^{\rm r}_{I_{\rm g2}}(s)=\exp\Big(-\frac{2\pi\lambda_{\rm g}\mu_{\rm g}sD^{2-\alpha_{\rm N}}}{\alpha_{\rm N}-2}F(\alpha_{\rm N},\mu_{\rm m}sD^{-\alpha_{\rm N}})+2\lambda_{\rm g}\int_{r_2}^{D+r}\frac{\arccos\left(\frac{r^2+t^2-D^2}{2rt}\right)t{\rm d}t}{1+(s\mu_{\rm g})^{-1}t^{\alpha_{\rm N}}}\Big),\tag{45}$$

where $r_2=\max(D,r-D)$. For the LT of $I_{\rm u}$, we adopt the PPP approximation and obtain

$$\begin{aligned}\mathcal{L}^{\rm r}_{I_{\rm u2}}(s)&\overset{(e)}{\approx}\mathbb{E}\Big[\prod_{y\in\Phi_{\rm PPP}\setminus b(o,r)}\sum_{i\in\{\rm L,N\}}\frac{P_i(\|y\|,h_y)}{\left(1+\frac{sG(\phi_y)\mu_{\rm u}}{M_i}(\|y\|^2+h_{\rm f}^2)^{-\alpha_i/2}\right)^{M_i}}\Big]\\&=\exp\Bigg(-2\pi\lambda_{\rm I}\sum_{i\in\{\rm L,N\}}\int_{h_{\min}}^{h_{\max}}f(u)P_i(t,u)\Big(\int_{r}^{u\tan\psi_{\rm m}}\Big(1-\frac{1}{(1+\frac{s\mu_{\rm u}G_{\rm m}}{M_i(t^2+u^2)^{\alpha_i/2}})^{M_i}}\Big)t{\rm d}t\\&\quad+\int_{u\tan\psi_{\rm m}}^{\infty}\Big(1-\frac{1}{(1+\frac{s\mu_{\rm u}G_{\rm s}}{M_i(t^2+u^2)^{\alpha_i/2}})^{M_i}}\Big)t{\rm d}t\Big){\rm d}u\Bigg),\end{aligned}\tag{46}$$

where $b(o,r)$ is excluded in step (e) since the interfering UAVs are farther than the serving UAV.

Finally, when the typical user is a GEU, we have $r>D$ and the LT of $I_{\rm g}$ is same as the GCU, namely, $\mathcal{L}^{\rm r}_{I_{\rm g3}}(s)=\mathcal{L}^{\rm r}_{I_{\rm g1}}(s)$. For $I_{\rm u}$, its LT is approximated by

$$\begin{aligned}\mathcal{L}^{\rm r}_{I_{\rm u3}}(s)&\overset{(f)}{\approx}\mathbb{E}\Big[\prod_{y\in\Phi_{\rm PPP}}\sum_{i\in\{\rm L,N\}}\frac{P_i(\|y\|,h_y)}{\left(1+\frac{sG(\phi_y)\mu_{\rm u}}{M_i}(\|y\|^2+h_{\rm f}^2)^{-\alpha_i/2}\right)^{M_i}}\mid\|y\|>h_y\tan\psi_{\rm m}\Big]\\&=\exp\Big(-2\pi\lambda_{\rm I}\sum_{i\in\{\rm L,N\}}\int_{h_{\min}}^{h_{\max}}\int_{u\tan\psi_{\rm m}}^{\infty}P_i(t,u)f(u)\Big(1-\frac{1}{(1+\frac{s\mu_{\rm u}G_{\rm s}}{M_i(t^2+u^2)^{\alpha_i/2}})^{M_i}}\Big)t{\rm d}t{\rm d}u\Big),\end{aligned}\tag{47}$$

where $b(o,R_y)$ is excluded in step (f) due to that the GUE is outside the UAV coverage region.

APPENDIX C
PROOF OF THEOREM 2

For the typical GCU, it is served by the nearest GBS, and we have

$$P_1^{\mathrm{r}}(\theta)=\mathbb{P}\Big(\frac{\mu_{\mathrm{g}}g_{x_0}\ell_{\mathrm{g}}(x_0)}{I_{\mathrm{g}}+I_{\mathrm{u}}}>\theta\mid o\in\mathcal{C}_1\Big)\overset{(a)}{=}\int_0^D\mathcal{L}^{\mathrm{f}}_{I_{\mathrm{g1}}}(\theta\mu_{\mathrm{g}}^{-1}r^{\alpha_{\mathrm{N}}})\mathcal{L}^{\mathrm{f}}_{I_{\mathrm{u1}}}(\theta\mu_{\mathrm{g}}^{-1}r^{\alpha_{\mathrm{N}}})f_1^{\mathrm{f}}(r)\mathrm{d}r,\tag{48}$$

where step (a) follows the Rayleigh fading for the NLOS link. For the typical UEU, we have

$$\begin{aligned}
P_2^{\mathrm{r}}(\theta)=&\mathbb{P}\Big(\frac{\mu_{\mathrm{u}}G_{\mathrm{m}}g_{y_0}\ell_{\mathrm{u}}(y_0)}{I_{\mathrm{g}}+I_{\mathrm{u}}}>\theta\mid o\in\mathcal{C}_2\Big)\\
=&\int_{h_{\min}}^{h_{\max}}\int_0^{u\tan\psi_{\mathrm{m}}}\sum_{i\in\{\mathrm{L},\mathrm{N}\}}P_i(r,u)\mathbb{E}\Big[\widetilde{\Gamma}\Big(M_i,\frac{M_i\theta(r^2+u^2)^{\alpha_i/2}}{G_{\mathrm{m}}\mu_{\mathrm{u}}}(I_{\mathrm{g}}+I_{\mathrm{u}})\Big)\Big]f_2^{\mathrm{r}}(r\mid h_{y_0}=u)\varrho_2^{\mathrm{r}}(u)\mathrm{d}r\mathrm{d}u\\
=&\int_{h_{\min}}^{h_{\max}}\int_0^{u\tan\psi_{\mathrm{m}}}\sum_{i\in\{\mathrm{L},\mathrm{N}\}}P_i(r,u)\sum_{l=0}^{M_i-1}\mathbb{E}\Big[e^{-\frac{M_i\theta(r^2+u^2)^{\alpha_i/2}}{G_{\mathrm{m}}\mu_{\mathrm{u}}}(I_{\mathrm{g}}+I_{\mathrm{u}})}\\
&\qquad\times\frac{\big(\frac{M_i\theta(r^2+u^2)^{\alpha_i/2}}{G_{\mathrm{m}}\mu_{\mathrm{u}}}(I_{\mathrm{g}}+I_{\mathrm{u}})\big)^l}{l!}\Big]f_2^{\mathrm{r}}(r\mid h_{y_0}=u)\varrho_2^{\mathrm{r}}(u)\mathrm{d}r\mathrm{d}u\\
=&\int_{h_{\min}}^{h_{\max}}\int_0^{u\tan\psi_{\mathrm{m}}}\sum_{i\in\{\mathrm{L},\mathrm{N}\}}P_i(r,u)\sum_{l=0}^{M_i-1}\frac{(-s)^l}{l!}\mathcal{L}^{(l)}(r,u,s)\mid_{s=\frac{M_i\theta(r^2+u^2)^{\alpha_i/2}}{G_{\mathrm{m}}\mu_{\mathrm{u}}}}f_2^{\mathrm{r}}(r\mid h_{y_0}=u)\varrho_2^{\mathrm{r}}(u)\mathrm{d}r\mathrm{d}u,
\end{aligned}$$

where $\mathcal{L}^{(l)}(r,u,s)=\mathbb{E}[e^{-s(I_{\mathrm{g}}+I_{\mathrm{u}})}]=\mathcal{L}^{\mathrm{r}}_{I_{\mathrm{g2}}}(s)\mathcal{L}^{\mathrm{r}}_{I_{\mathrm{u2}}}(s)$ is the LT of $I_{\mathrm{g}}+I_{\mathrm{u}}$ under the condition that the serving UAV is at a distance r and altitude u, and the superscript (l) stands for the l-th derivative of $\mathcal{L}^{(l)}(r,u,s)$ w.r.t. s. For the typical GEU, the SIR CCDF is obtained similarly.

REFERENCES

[1] N. Deng, L. Chen, and H. Wei, "A 3D UAV-assisted cellular network model with inter-tier dependence," in *IEEE Wireless Communications and Networking Conference (WCNC'21)*, Nanjing, China, March 2021.

[2] N. Cheng, W. Xu, W. Shi, Y. Zhou, N. Lu, H. Zhou, and X. Shen, "Air-ground integrated mobile edge networks: Architecture, challenges, and opportunities," *IEEE Communications Magazine*, vol. 56, no. 8, pp. 26–32, Aug. 2018.

[3] J. Qiu, D. Grace, G. Ding, M. D. Zakaria, and Q. Wu, "Air-ground heterogeneous networks for 5G and beyond via integrating high and low altitude platforms," *IEEE Wireless Communications*, vol. 26, no. 6, pp. 140–148, Dec. 2019.

[4] M. Mozaffari, W. Saad, M. Bennis, Y.-H. Nam, and M. Debbah, "A tutorial on UAVs for wireless networks: Applications, challenges, and open problems," *IEEE Communications Surveys & Tutorials*, vol. 21, no. 3, pp. 2334–2360, Third quarter 2019.

[5] X. Lu, M. Salehi, M. Haenggi, E. Hossain, and H. Jiang, "Stochastic geometry analysis of spatial-temporal performance in wireless networks: A tutorial," *IEEE Communications Surveys & Tutorials*, vol. 23, no. 4, pp. 2753–2801, Fourth quarter 2021.

[6] X. Xu and Y. Zeng, "Cellular-connected UAV: Performance analysis with 3D antenna modelling," in *2019 IEEE International Conference on Communications Workshops (ICC Workshops)*, Shanghai, China, May 2019.

[7] Y. Du, H. Zhang, and J. Peng, "Modelling and coverage analysis for cellular-connected UAVs with up-tilted antenna," *IEEE Communications Letters*, 2022, IEEE Early Access.

[8] T. Hou, Y. Liu, Z. Song, X. Sun, and Y. Chen, "NOMA-enhanced terrestrial and aerial IoT networks with partial CSI," *IEEE Internet of Things Journal*, vol. 7, no. 4, pp. 3254–3266, April 2020.

[9] N. Senadhira, S. Durrani, X. Zhou, N. Yang, and M. Ding, "Uplink NOMA for cellular-connected UAV: Impact of UAV trajectories and altitude," *IEEE Transactions on Communications*, vol. 68, no. 8, pp. 5242–5258, Aug. 2020.

[10] W. K. New, C. Y. Leow, K. Navaie, Y. Sun, and Z. Ding, "Interference-aware NOMA for cellular-connected UAVs: Stochastic geometry analysis," *IEEE Journal on Selected Areas in Communications*, vol. 39, no. 10, pp. 3067–3080, Oct. 2021.

[11] V. V. Chetlur and H. S. Dhillon, "Downlink coverage analysis for a finite 3-D wireless network of unmanned aerial vehicles," *IEEE Transactions on Communications*, vol. 65, no. 10, pp. 4543–4558, Oct. 2017.

[12] S. Zhang, J. Liu, and W. Sun, "Stochastic geometric analysis of multiple unmanned aerial vehicle-assisted communications over Internet of Things," *IEEE Internet of Things Journal*, vol. 6, no. 3, pp. 5446–5460, June 2019.

[13] W. Yi, Y. Liu, Y. Deng, and A. Nallanathan, "Clustered UAV networks with millimeter wave communications: A stochastic geometry view," *IEEE Transactions on Communications*, vol. 68, no. 7, pp. 4342–4357, July 2020.

[14] Y. Qin, M. A. Kishk, and M.-S. Alouini, "Performance evaluation of UAV-enabled cellular networks with battery-limited drones," *IEEE Communications Letters*, vol. 24, no. 12, pp. 2664–2668, Dec. 2020.

[15] R. Jiang, K. Xiong, H.-C. Yang, P. Fan, Z. Zhong, and K. B. Letaief, "On the coverage of UAV-assisted SWIPT networks with nonlinear EH model," *IEEE Transactions on Wireless Communications*, vol. 21, no. 6, pp. 4464–4481, June 2021.

[16] Y. Sun, Z. Ding, and X. Dai, "A user-centric cooperative scheme for UAV-assisted wireless networks in malfunction areas," *IEEE Transactions on Communications*, vol. 67, no. 12, pp. 8786–8800, Dec. 2019.

[17] X. Wang, H. Zhang, Y. Tian, and V. C. M. Leung, "Modeling and analysis of aerial base station-assisted cellular networks in finite areas under LoS and NLoS propagation," *IEEE Transactions on Wireless Communications*, vol. 17, no. 10, pp. 6985–7000, Oct. 2018.

[18] N. Kouzayha, H. Elsawy, H. Dahrouj, K. Alshaikh, T. Y. Al-Naffouri, and M.-S. Alouini, "Analysis of large scale aerial terrestrial networks with mmWave backhauling," *IEEE Transactions on Wireless Communications*, vol. 20, no. 12, pp. 8362–8380, Dec. 2021.

[19] M. Alzenad and H. Yanikomeroglu, "Coverage and rate analysis for vertical heterogeneous networks (VHetNets)," *IEEE Transactions on Wireless Communications*, vol. 18, no. 12, pp. 5643–5657, Dec. 2019.

[20] M. M. Azari, G. Geraci, A. Garcia-Rodriguez, and S. Pollin, "UAV-to-UAV communications in cellular networks," *IEEE Transactions on Wireless Communications*, vol. 19, no. 9, pp. 6130–6144, Sept. 2020.

[21] Y. Jiang, Z. Fei, J. Guo, and Q. Cui, "Coverage performance of the terrestrial-UAV HetNet utilizing licensed and unlicensed spectrum bands," *IEEE Access*, vol. 9, pp. 124 100–124 114, Sept. 2021.

[22] D. Kim, J. Lee, and T. Q. S. Quek, "Multi-layer unmanned aerial vehicle networks: Modeling and performance analysis," *IEEE Transactions on Wireless Communications*, vol. 19, no. 1, pp. 325–339, 2020.

[23] A. M. Hayajneh, S. A. R. Zaidi, D. C. McLernon, M. Di Renzo, and M. Ghogho, "Performance analysis of UAV enabled disaster recovery networks: A stochastic geometric framework based on cluster processes," *IEEE Access*, vol. 6, pp. 26 215–26 230, May 2018.

[24] P. Ji, X. Jia, Y. Lu, H. Hu, and Y. Ouyang, "Multi-UAV assisted multi-tier millimeter-wave cellular networks for hotspots

with 2-tier and 4-tier network association," *IEEE Access*, vol. 8, pp. 158 972–158 995, Aug. 2020.

[25] Z. Chen and H. Zhang, "UAV-assisted networks through a tunable dependent model," *IEEE Communications Letters*, vol. 24, no. 5, pp. 1110–1114, May 2020.

[26] X. Guo, C. Zhang, F. Yu, and H. Chen, "Coverage analysis for UAV-assisted mmwave cellular networks using Poisson hole process," *IEEE Transactions on Vehicular Technology*, vol. 71, no. 3, pp. 3171–3186, March 2022.

[27] M. Haenggi. How well do distributions match? A case for the MH distance. [Online]. Available: https://stogblog.net/2022/06/15/how-well-do-distributions-match-a-case-for-the-mh-distance/

[28] J. G. Andrews, T. Bai, M. N. Kulkarni, A. Alkhateeb, A. K. Gupta, and R. W. Heath, "Modeling and analyzing millimeter wave cellular systems," *IEEE Transactions on Communications*, vol. 65, no. 1, pp. 403–430, 2017.

[29] M. Haenggi, *Stochastic geometry for wireless networks*. Cambridge University Press, 2012.

[30] A. Al-Hourani, S. Kandeepan, and S. Lardner, "Optimal LAP altitude for maximum coverage," *IEEE Wireless Communications Letters*, vol. 3, no. 6, pp. 569–572, Dec. 2014.

[31] A. Fotouhi, H. Qiang, M. Ding, M. Hassan, L. G. Giordano, A. Garcia-Rodriguez, and J. Yuan, "Survey on UAV cellular communications: Practical aspects, standardization advancements, regulation, and security challenges," *IEEE Communications Surveys & Tutorials*, vol. 21, no. 4, pp. 3417–3442, Fourth quarter 2019.

[32] A. Rajanna and M. Haenggi, "Enhanced cellular coverage and throughput using rateless codes," *IEEE Transactions on Communications*, vol. 65, no. 5, pp. 1899–1912, May 2017.

[33] N. Deng and M. Haenggi, "The end-to-end performance of rateless codes in Poisson bipolar and cellular networks," *IEEE Transactions on Communications*, vol. 67, no. 11, pp. 8072–8085, Aug. 2019.

[34] N. Deng, W. Zhou, and M. Haenggi, "Heterogeneous cellular network models with dependence," *IEEE Journal on Selected Areas in Communications*, vol. 33, no. 10, pp. 2167–2181, Oct. 2015.

[35] Z. Yazdanshenasan, H. S. Dhillon, M. Afshang, and P. H. J. Chong, "Poisson hole process: Theory and applications to wireless networks," *IEEE Transactions on Wireless Communications*, vol. 15, no. 11, pp. 7531–7546, Nov. 2016.

[36] N. Deng, M. Haenggi, and Y. Sun, "Millimeter-wave device-to-device networks with heterogeneous antenna arrays," *IEEE Transactions on Communications*, vol. 66, no. 9, pp. 4271–4285, Sept. 2018.

[37] H. Alzer, "On some inequalities for the incomplete gamma function," *Mathematics of Computation*, vol. 66, no. 218, pp. 771–778, 1997.

[38] M. Haenggi, "SIR analysis via signal fractions," *IEEE Communications Letters*, vol. 24, no. 7, pp. 1358–1362, July 2020.